# Dry etching in the presence of physisorption of neutrals at lower temperatures $\odot \bigcirc$

Thorsten Lill **№ (**0); Ivan L. Berry **(**0); Meihua Shen; John Hoang **(**0); Andreas Fischer **(**0); Theo Panagopoulos **(**0); Jane P. Chang **(**0); Vahid Vahedi



Journal of Vacuum Science & Technology A 41, 023005 (2023)

https://doi.org/10.1116/6.0002230





CrossMark



# Dry etching in the presence of physisorption of neutrals at lower temperatures

Cite as: J. Vac. Sci. Technol. A 41, 023005 (2023); doi: 10.1116/6.0002230 Submitted: 16 September 2022 · Accepted: 20 January 2023 · Published Online: 27 February 2023







Thorsten Lill, <sup>1,a)</sup> 🗓 Ivan L. Berry, ¹ 🗓 Meihua Shen, ¹ John Hoang, ¹ 🗓 Andreas Fischer, ¹ 🗓 Theo Panagopoulos, ¹ 🗓 Jane P. Chang,² 匝 and Vahid Vahedi¹

#### **AFFILIATIONS**

- <sup>1</sup>Lam Research Corporation, 4400 Cushing Parkway, Fremont, California 94538
- <sup>2</sup>Department of Chemical and Biomolecular Engineering, University of California Los Angeles, Los Angeles, California 90095

#### **ABSTRACT**

In this article, we give an overview about the chemical and physical processes that play a role in etching at lower wafer temperatures. Conventionally, plasma etching processes rely on the formation of radicals, which readily chemisorb at the surface. Molecules adsorb via physisorption at low temperatures, but they lack enough energy to overcome the energy barrier for a chemical reaction. The density of radicals in a typical plasma used in semiconductor manufacturing is one to two orders of magnitude lower than the concentration of the neutrals. Physisorption of neutrals at low temperatures, therefore, increases the neutral concentration on the surface meaningfully and trals. Physisorption of neutrals at low temperatures, therefore, increases the neutral concentration on the surface meaningfully and contributes to etching if they are chemically activated. The transport of neutrals in high aspect ratio features is enhanced at low temperatures of how temperatures are the increase of the contributes to etching if they are chemically activated. The transport of neutrals in high aspect ratio features is enhanced at low temperatures of how temperatures are the increase of the contributes to etching if they are chemically activated. because physisorbed species are mobile. The temperature window of low temperature etching is bracketed at the low end by condensation including capillary effects and diminished physisorption at the high end. The useful temperature window is chemistry dependent. Besides illuminating the fundamental effects, which make low temperature processing unique, this article illustrates its utility for semiconductor etching applications.

Published under an exclusive license by the AVS. https://doi.org/10.1116/6.0002230

# I. INTRODUCTION

In the manufacturing of integrated circuits, etching and deposition processes with and without plasma are widely used. Except for physical processes such as physical vapor deposition and ion beam etching, these processes leverage the adsorption of reactive species to enable chemical reactions at the wafer surface. Adsorption is the attachment or adhesion of atoms or molecules from a gas to a solid surface. If they form chemical bonds, the process is called chemisorption. The chemisorption of reactive neutral species weakens the bonds at the surface and allows for more efficient removal by thermal energy or ion bombardment. Neutral species are atoms and molecules without electric charge. If these neutrals have at least one unpaired valence electron, they are called radicals. The chemical weakening of the surface is critical for chemical or chemically enhanced etching processes such as thermal etching, radical etching, atomic layer etching (ALE), and reactive ion etching (RIE).

In this article, we review a process regime, which is frequently referred to as low temperature etching<sup>2-6</sup> or "cryogenic" etching. Today, this term is loosely applied to etching processes below 0 °C. The delineation arrives from the need for special hardware to cool the wafer and to avoid condensation inside the tool. However, important effects are observed depending on pressure and chemical nature of the gases and surfaces at temperatures, which may not be below 0 °C. 10,11 They are caused by a transition from chemisorption to physisorption, which is defined as a process in which chemical bonds are not formed upon adsorption. Implications include a higher neutral concentration on the surface and higher etching rates due to physisorption of undissociated neutral species. Enhanced adsorption of etching by-products enables profile control without the addition of polymerizing gases.<sup>2-4</sup> The experimental results for high aspect ratio features show that aspect ratio dependent etching (ARDE) can be reduced. 12 One of the potential explanations is that surface diffusion is emerging as an important transport mechanism for neutral species. Multilayer adsorption and capillary condensation have been shown to reduce plasma damage in porous low-k materials. 13

These unique properties of low temperature etching are documented in the literature starting from the late 1980s.

a)Author to whom correspondence should be addressed: thorsten.lill@lamreserach.com

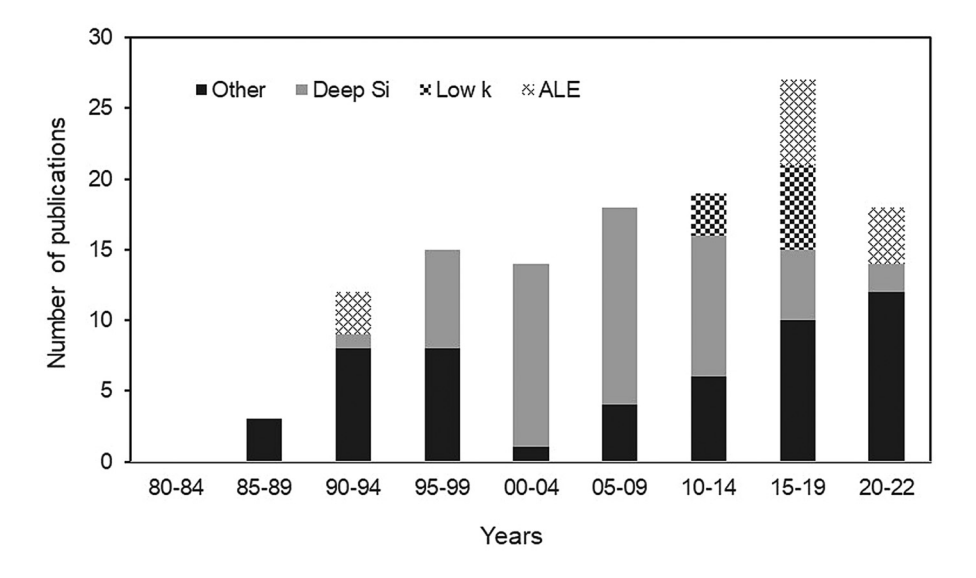


FIG. 1. Chronology of the number of publications on low

Figure 1 shows the chronology of the number of publications on low temperature etching. We included all available articles on reactive ion etching, atomic layer etching, and ion or electron beam etching at temperatures below 0 °C and higher temperatures if physisorption was demonstrated to play a role. A continuous increase in the number of publications can be observed. For the first 25 years starting with Tachi's seminal paper on low temperature silicon etching,<sup>2</sup> research was focused on silicon etching with fluorine and high aspect ratio etching of silicon. 3-9,12,1second wave of interest started around 2013 with articles on porous low-k etching, <sup>10,11,13,55-60</sup> application of physisorption to atomic layer etching, <sup>61-68</sup> etching of silicon features with dimensions below 20 nm, <sup>69-78</sup> and etching of silicon nitride. <sup>79,80</sup> As conventional etching of 3D NAND devices faces challenges, low temperature etching is being introduced into production for high aspect ratio dielectric patterning. 81-83 In May 2022, the First International Workshop on Plasma Cryogenic Etching Processes was held in Orleans, France. Low temperature etching appears at the cusp of wider use in the semiconductor industry. This article intends to illuminate the fundamental effects, which make low temperature processing unique, and to illustrate its utility for semiconductor etching applications.

#### II. FUNDAMENTALS

#### A. Etching rates

The etching rate for RIE with ideal ion-neutral synergy can be expressed by the following formula:8

$$ER = \frac{vE_iJ_i}{1 + vE_iJ_i/(v_nsJ_n)},\tag{1}$$

where  $E_i$  is the average ion energy,  $J_i$  is the ion flux, and v is the volume of the material removed per unit bombardment energy for a saturated surface. The product of these three parameters represents the etch rate in the ion limited regime for a synergistic etch process. The etch rate in a neutral flux limited regime is the product of the neutral flux  $J_n$ , the reactive sticking probability s, and the volume removed per reactive neutral  $v_n$ . Conventional RIE utilizes chemically active neutral species to chemisorb and to weaken the bonds at the surface. The value of  $v_n$  is dependent on the ion energy because of the correlation between deposited energy and the number of broken bonds at the surface, which facilitate the o chemisorption of neutrals.

Molecules and atoms can also stick to surfaces without forming chemical bonds. This process is called physisorption. All gases physisorb at low enough surface temperatures. They stick to the surface via van der Waal's forces, which are classified by the interaction between the surface and the molecule or atom.85 Among these forces, the London dispersion force is the weakest intermolecular force. It is an induced dipole-induced dipole attraction and happens between transient, nonpermanent dipoles. Next, ion-dipole forces exist when the solid surface has ionic bonds, and the molecule is polar. Similarly, ion-induced dipole forces exist between ionic surfaces and polarizable gas molecules. Forces between polar surfaces and polar molecules are called dipole forces. Finally, van der Waals forces also result from quadrupole interactions. In general, van der Waals forces and the process of physisorption are determined by the chemical nature of the surface and gas species.

Molecules are physisorbed mostly without an activation barrier. The binding energy  $E_{ads, phys}$  is small, typically less than 0.5 eV as shown in Table I. This favors physisorption at low surface temperatures. The incoming molecule must also lose excess kinetic energy to the lattice of the solid surface to prevent reflection. This process is also favored at lower surface temperatures. Physisorption is an intermediate step for chemisorption. The Lennard-Jones graph in Fig. 2 illustrates this. When a physisorbed molecule overcomes an activation energy  $E_a$ , it forms chemical bonds with an energy of  $E_{ads, chem}$ , which is about one order of magnitude larger than the physisorption energy,  $E_{ads, phys}$ . 87 This activation energy is the reason why chemisorption is favored at higher surface temperatures. Figure 2 shows

**TABLE I.** Physisorption energies of gases on surfaces used in semiconductor device manufacturing. References are given in superscripts. All values are calculated using density functional theory (DFT) except from Ref. 88, which is an experimental value. In the DFT calculations, the silicon surface is terminated with hydrogen and the silicon oxide surface with hydroxyl.

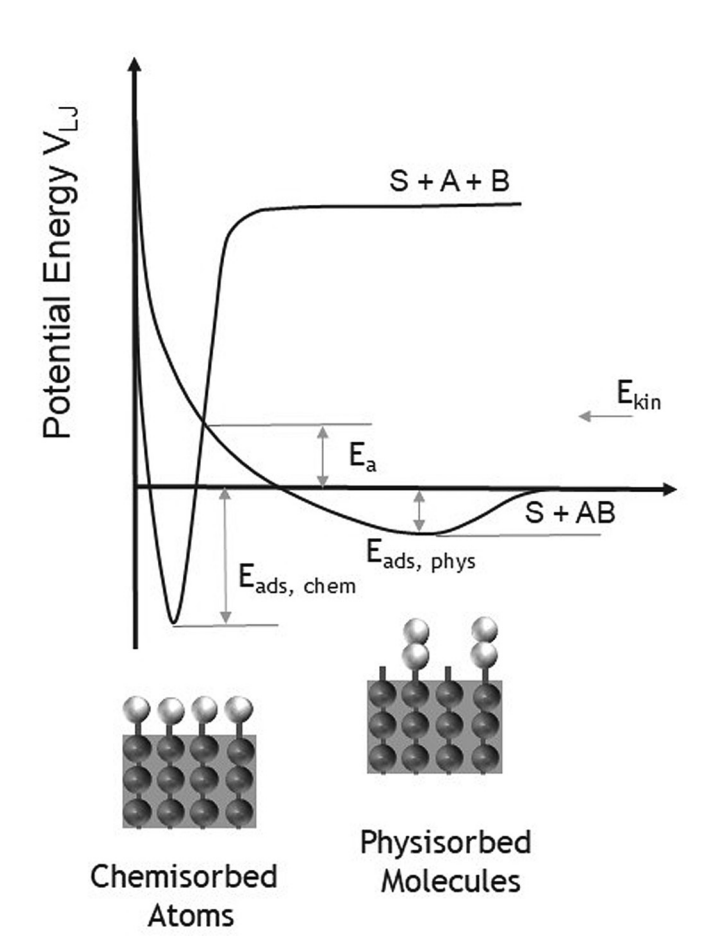
	$E_{ads,phys}$ (eV)						
	CF <sub>4</sub>	CHF <sub>3</sub>	$CH_2F_2$	CH <sub>3</sub> F	CIF <sub>3</sub>	NF <sub>3</sub>	HF
Si	0.7189	0.1889			$0.29^{89}$ $0.06^{88}$	0.7089	0.13 <sup>89</sup>
$\begin{array}{c} SiO_2 \\ Si_3N_4 \end{array}$	0.26 <sup>89</sup> 0.22 <sup>90</sup>		0.12 <sup>90</sup>	$0.61^{90}$ $0.20^{91}$ $0.22^{90}$	0.16 <sup>89</sup>	0.16 <sup>89</sup>	0.53 <sup>89</sup> 1.02 <sup>90</sup>

that the molecule dissociates in the process, which is not always the case. Molecules can also chemisorb without dissociating.

The Lennard–Jones graph in Fig. 2 also helps to explain the isobars for physisorption and chemisorption shown in Fig. 3. As the surface temperature decreases, more molecules are physisorbed to the surface because its temperature is low enough for them to stay trapped in the shallow physisorption energy minimum [Fig. 3(a)]. Initially, this leads also to more chemisorbed molecules so long as

the energy of the system is high enough that the activation barrier can be crossed. As the temperature is further decreased, there is decreasing coverage of chemisorbed molecules as shown in the inset in Fig. 3(b). At exceedingly high temperatures, few molecules physisorb, which also causes a decreasing coverage of chemisorbed molecules.

Table II lists the salient characteristics of physisorption and chemisorption. Physisorption can reverse at constant temperature and reduced pressure (isothermal reversibility). This process is slow or absent for chemisorption. This has important implications for cyclic processes such as ALE and atomic layer deposition (ALD) where gases change between steps. Chemisorbed species form strong bonds with the surface, which weakens bonds between surface atoms. This effect is enabling chemical and chemically assisted etching processes. Physisorbed species do not cause structural changes to the surface. The bonds between the surface atoms remain unchanged. Therefore, physisorbed species require the external energy provided by accelerated ions, electrons, or photons to stimulate chemical reactions and to aid in the etching process. Physisorbed species can form multilayer structures because the same forces are well known to lead to the condensation of vapors. At high enough pressures and low enough temperatures, gases can condense at the surface.



Distance r

**FIG. 2.** Lennard–Jones graph describing dissociative adsorption of a diatomic molecule AB on a surface S.



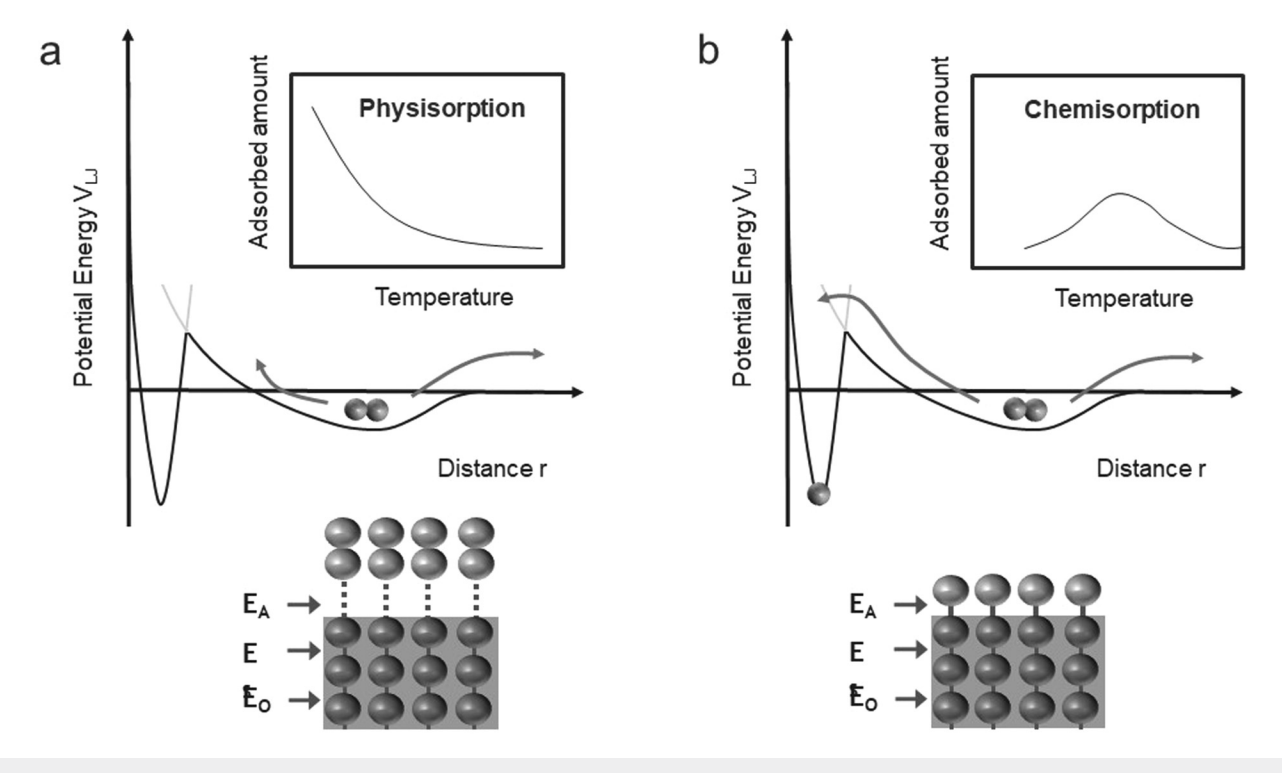


FIG. 3. Schematic illustration of physisorption (a) and chemisorption (b) and their corresponding isobars.

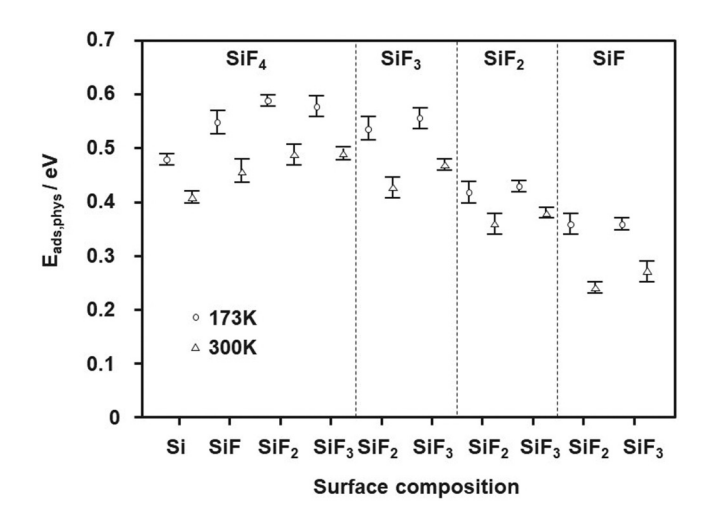
The type of plasma that is used in dry etching is called low temperature or nonequilibrium plasma. P2-94 Charged species are lost to the wall faster than they are able to transfer via collisions with neutrals the energy they receive from an external energy source. Hence, the neutrals are colder than the ions. Molecules and atoms approach the surface with a kinetic energy given by the temperature of the background gas. Typical background gas temperatures are in the range between 300 and 2000 K or 0.03 and 0.15 eV. P2.95.96 This is on average smaller than the desorption energies listed in Tables I and II. Also, there is a meaningful temperature difference between the reactor walls and the bulk gas at the

TABLE II. Comparison between physisorption and chemisorption.

Property	Physisorption	Chemisorption
Forces	van der Waals	Chemical bonding
Binding energy,		_
$E_{ads}$ (eV)	< 0.5	>2.0
Activation energy,		
$E_a$ (eV)	Rare	0.6-1.0
Isothermal		
reversibility	Complete	Slow or none
Interaction	No structural	Disruption of chemical
	changes	bonds possible
Extend	Multilayers	Monolayer

pressures used in typical RIE processes, which are typically below 50 mTorr. The gas temperature above a low temperature cathode should be lower than typically expected values. This ensures that approaching gas species are trapped at the surface if they lose energy in the collision with the surface.

The wafer surface is heated by the background gas and ion impacts. While the peak power density per ion impact is very high (10<sup>8</sup>-10<sup>12</sup> W/cm<sup>2</sup>) and causes collision cascades and sputtering, the average power delivered to the wafer is low (10<sup>4</sup> W/cm<sup>2</sup> for an ion energy of 100 eV and an ion current density of 10 mA/cm<sup>2</sup>). Therefore, the wafer surface can be etched without excessive thermal impact.<sup>92</sup> The heat generated by the plasma on the wafer must still be removed with a wafer cooling mechanism, typically an electrostatic chuck (ESC). In the following discussion, we refer to the wafer surface temperatures, assuming cooling by an ESC. Experiments on different surfaces have shown that chemisorption does not occur or only proceeds slowly at room temperature for many etch gases such as CF<sub>4</sub>, CF<sub>3</sub>H, CF<sub>2</sub>Cl<sub>2</sub>, and CCl<sub>4</sub>. One of the roles plasma plays in RIE is to dissociate nonreactive molecules into reactive species or radicals, which readily chemisorb. The density of radicals in a typical low temperature plasma is one to two orders of magnitude lower than that of the background gas. Trapping nondissociated neutral species using physisorption at low surface temperatures, therefore, increases their concentration on the surface. Since RIE utilizes the synergy between ion and neutral species,<sup>98</sup> larger neutral surface concentrations enable higher etching rates.



**FIG. 4.** Physisorption energies for  $SiF_x$  on fluorinated silicon. Reprinted with permission from Tinck *et al.*, J. Phys. Chem. C **118**, 30315 (2014). Copyright 2014, American Chemical Society.

Physisorbed species desorb at a rate  $R_{des}$ , which depends on the surface temperature T, the physisorption energy  $E_{ads,phys}$ , and the surface coverage  $\theta$ ,

$$R_{des} = k_0 e^{-E_{ads.phys}/k_b T} \theta, (2)$$

where  $k_b$  is the Boltzmann constant and  $k_0$  is a rate constant, which depends on surface properties including defects and roughness. Equation (2) shows that species remain on the surface for a longer time if the physisorption energy is higher and/or the surface temperature is lower.

Of the molecules listed in Table I, the highest  $E_{ads,phys}$  for OH terminated SiO<sub>2</sub> is observed for CH<sub>3</sub>F, while CF<sub>4</sub> has the largest physisorption energy for hydrogen terminated silicon and HF for Si<sub>3</sub>N<sub>4</sub>. This illustrates the importance of chemistry for physisorption.

Tinck et al. calculated  $E_{ads, phys}$  for various  $SiF_x$  species on fluorinated silicon<sup>99</sup> using molecular dynamics methods. One important insight from their work is that radicals can also physisorb.

The authors found that F, Si, and F<sub>2</sub> always quickly chemisorb or reflect after impact. Figure 4 depicts the physisorption energies for the other surface/molecule combinations for temperatures of 173 and 300 K. The adsorption energies are higher for 173 K. The authors explained this with smaller oscillation amplitudes between adsorbent and surface at lower temperatures, leading to slightly smaller average physisorption bond lengths and, hence, to overall stronger van der Waals forces. This effect would further enhance the temperature sensitivity of the desorption rate in Eq. (2). Figure 4 shows that the energy needed for desorption decreases with decreasing size of the species. The degree of fluorination appears less important for the systems studied in this work.

In most applications, mixtures of gases are used to etch semi-conductor devices. These gases can co-adsorb and interact. Attractive interactions between the species raise and repulsive ones lower  $E_{ads,\,phys.}^{100}$ 

# **B.** Activation of chemical processes

Physisorbed species must be activated by external energy to chemisorb and facilitate the removal of surface atoms. Figure 2 shows that chemisorption occurs when a physisorbed molecule gathers kinetic energy, which is larger than the sum of the physisorption energy  $E_{ads,phys}$  and the activation barrier for chemisorption  $E_a$ . For desorption, only  $E_{ads,phys}$  is needed, which means that there is a large probability that species desorb rather than chemisorb. There is still a probability for chemisorption because of reaction kinetics. The activation efficiency, therefore, depends on the type of activation. Table III lists different activation species and mechanisms. These species are generated in plasmas.

Surface ion impacts are separated in time for low temperature plasmas. The energy from one impact does not overlap with other impacts. While the wafer is kept at low temperature via backside cooling, the surface is amorphized via a collision cascade upon ion impact. This provides abundant thermal energy for dissociation and chemisorption fragments in the vicinity of the impact site. Winters proposed another mechanism where argon bombardment produces lattice damage, which enhances the spontaneous reaction between  $XeF_2$  and tungsten. Yet another potential mechanism is dissociation and chemisorption from direct impact by an ion or fast neutral. This effect is called collision induced dissociative chemisorption of adsorbates. Molecular beam techniques coupled with ultrahigh vacuum electron spectroscopy have been

TABLE III. Species and mechanisms for chemical activation of physisorbed species in low temperature etching.

Activation species	Experimental techniques	Activation mechanisms
Ions and fast	Atomic layer etching with ion removal step $^{64-67,101,102}$ Ion beam experiments $^{104-109}$	Local temperature at impact site 92,103 Direct impact dissociation of adsorbate 104-106
neutrals	Ion beam experiments 104-109	Direct impact dissociation of adsorbate 104-106
		Ion generated surface defects and dangling bonds 110-114
Electrons	Electron beam experiments <sup>88,98,115–118</sup>	Direct dissociation of adsorbate and chemisorption of fragments 116
	-	Electron generated surface defects and dangling bonds <sup>98</sup>
Photons	Laser beam experiments <sup>119</sup>	Direct dissociation of adsorbate and chemisorption of fragments
	Plasma experiments <sup>120</sup>	Photon generated charge carriers 119
	- -	Photon generated surface defects and dangling bonds

used to identify dissociation and chemisorption of  ${\rm CH_3}^{104}$  and desorption of  ${\rm CH_4}^{105}$  physisorbed on Ni at 46 K induced by the collision with an incident Ar atom with energies between 1.5 and 5 eV. This mechanism is most likely not applicable for ions with energies of several 100 eV.

Etching with neutral gases and electrons was demonstrated around the same time as ion based RIE and ALE. 98,108,115,118 In these early reports, the surface was at room temperature and the main effect of electrons was likely to stimulate the desorption of reaction products. The electron stimulated dissociation of adsorbed molecular hydrogen and etching of silicon was reported by Veprek and Sarott. 116 The reaction yield per electron reaches a maximum at a temperature of 60 °C. Above this temperature, it displays an Arrhenius-like dependence with a negative activation energy, which is attributed to the decrease of the surface coverage of physisorbed H<sub>2</sub>. Coburn and Winters suggested the formation of metallic silicon on the surface of SiO<sub>2</sub> under electron bombardment, which can be etched spontaneously by fluorine from XeF<sub>2</sub>. 98 More generally, this mechanism can be characterized as electron stimulated defect and dangling bond formation. Finally, electrons can heat the surface and promote the chemisorption of physisorbed molecules.

The mechanisms for chemisorption via photon and electron activation are similar. They include direct dissociation of adsorbate and chemisorption of fragments,  $^{121}$  photon generated surface defects and dangling bond, and an increase in wafer temperature. Houle reported the results on the photochemical etching of silicon with XeF $_2$  and explained the results evoking the effect of photogenerated charge carriers.  $^{119}$  Shin  $\it et~al.$  observed the photoassisted etching of silicon in a chlorine plasma.  $^{120}$ 

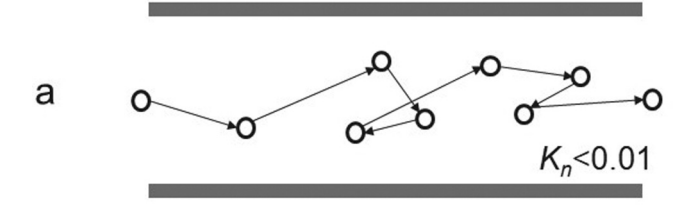
Finally, we can also consider the possibility to expose physisorbed molecules to neutral molecules or radicals to stimulate etching. We did not find literature sources for such a mechanism.

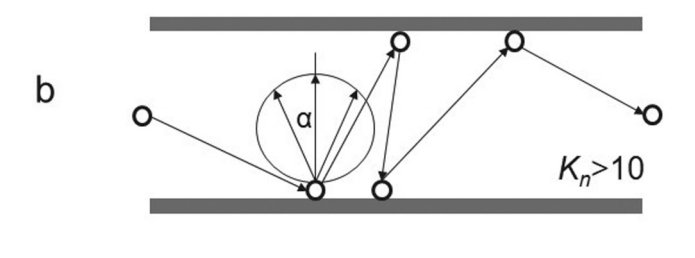
# C. Aspect ratio dependent etching (ARDE)

Etching rates generally decrease as feature aspect ratios increase. This effect is called aspect ratio dependent etching (ARDE). ARDE is caused by the impairment of ion and neutral transport as can be deduced from Eq. (1). Gottscho *et al.* identified salient ARDE mechanisms for conventional RIE: Knudsen transport of neutrals inside the feature, neutral shadowing, ion shadowing, and differential charging of insulating microstructures. <sup>84</sup> Ion transport is surface temperature independent. Let us, therefore, explore the effect of surface temperature on neutral transport. Neutral transport in a structure during etching is analogous to gas flow in pores.  $K_N$ , the dimensional Knudsen number, is used to classify different flow mechanisms. It is the ratio of the mean free path  $\lambda$  of the gas molecules and the radius of the pore or contact hole, <sup>122</sup>

$$K_N = \frac{\lambda}{r}. (3)$$

Figure 5 depicts the gas transport through a hole or cylinder at different pressures and cylinder diameters. Figure 5(a) depicts the viscous flow or Fick's diffusion at high pressures and for large diameters, where the Knudsen number is less than about 0.01.





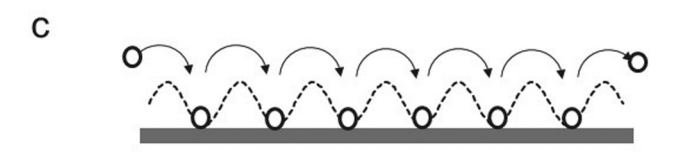


FIG. 5. Schematic illustration of Fick' diffusion (a), Knudsen transport (b), and surface diffusion (c).

01 August 2023 18:09:13

However, for dry etching of semiconductor devices, where pressures are low and dimensions are small, Knudsen numbers are much greater than 10, and free molecular flow prevails as illustrated in Fig. 5(b). The mean free path of argon at a pressure of 20 mTorr and the gas temperature of 500 K is 5 mm. Under these conditions, gas molecules rarely strike other molecules and instead collide with the cylinder walls of features with a cross section in the range of nanometers. This mechanism is known as molecular flow or Knudsen transport. 123 The RIE etching of large MEMS devices can operate at pressures large enough to reach a transition regime between viscous and Knudsen flow called slip flow with Knudsen numbers between 0.1 and 0.001. The Knudsen number for the etching of a MEMS structure with 4000 nm diameter using SF<sub>6</sub> at a pressure of 200 mTorr and a gas temperature of 500 K is 0.1. For slip flow, the viscous flow condition, which requires the average velocity of gas molecules directly adjacent to the wall to be equal to wall velocity, is no longer valid. The gas molecules slip at the solid wall. 124 Maxwell introduced a slip term to describe the flow of rarefied gases, which takes into consideration the number of molecules and atoms, which are reflected diffusively, which means by adsorbing and desorbing vs those which are reflected specularly. 125 For specular reflection, the emerging molecules and atoms maintain some of the characteristics they had before impact. The discussion



of the slip conditions is closely related to the molecule-surface interaction. A detailed general and complete description of these phenomena can be found, for instance, in Loeb's book "The Kinetic Theory of Gases."

Physisorbed species do not form chemical bonds. A molecule or atom attached to the surface by van der Waals forces diffuses across the surface until it chemisorbs or until it gains enough kinetic energy to desorb. This process is known as surface diffusion and is illustrated in Fig. 5(c).

Coburn and Winters identified Knudsen transport as the main neutral transport mechanism in conventional RIE. 127 It is one of the mechanisms causing the slowing of the etch rate as the aspect ratio increases.<sup>84</sup> During Knudsen diffusion inside a tube or cylinder, molecules hit a wall, oscillate in their potential wells, and desorb in a direction that is independent of their arrival angle as shown in Fig. 5(b).

Knudsen's theory of transport assumes that all molecules and atoms are reflected diffusively. The gas species lose their original direction and are emitted with a probability proportional to  $\cos \alpha$ . To explain this, Lorentz assumed that the walls of the pipe are molecularly rough. 128 Knudsen flow requires that a molecule striking the wall of a capillary must be held by some mechanism for a sufficient period to eliminate all effects of its direction of impact. Particles not scattering at 90° have as much likelihood of going forward through the tube as going backward toward the source. The Knudsen flux arriving at the bottom of a cylinder can be written as

$$J_K = c_K \Delta P, \tag{4}$$

where  $\Delta P$  is the pressure difference at the top and bottom of the feature. The unit of  $J_K$  is  $Pa^*m^{3*}s^{-1}$ , which represents the gas throughput. To obtain the molecular flow in  $s^{-1}$ , the term must be divided by  $k_b N_A T$ , where  $k_b$  is the Boltzmann constant,  $N_A$  is the Avogadro constant, and T is the gas temperature. The coefficient  $c_K$ is called molecular flow conductance. It is proportional to the velocity of the gas molecules. This implies a certain wafer temperature sensitivity if the molecules change their temperature in the interaction with the surface. The molecular flow conductance  $c_K$  is also proportional to the cross section of the tube and the transmission probability k. Clausing calculated k, assuming a molecule travels through a tube encountering diffuse collisions with the walls. 131 The results have been tabulated for the tubes of various shapes. 122,1

Coburn and Winters analyzed the neutral flows on the top,  $J_t$ , and bottom,  $J_b$ , of an etching feature as a function of the transmission probability k and reactive sticking coefficient s,

$$J_t - (1 - k)J_t - k(1 - s)J_b = sJ_b, (5)$$

where the second term represents the fraction of molecules, which are reflected out of the feature. The difference between the first and the second terms is the Knudsen flux at the bottom of the feature. The third term represents the molecules that reach the bottom but do not react and eventually escape out of the feature. The term on the right-hand side of the equation represents the species that are consumed by the etching of the bottom surface. For a sticking coefficient of 1, we get

$$J_b = J_K = kJ_t. (6)$$

For a sticking coefficient of 0, one obtains

$$k(J_t - J_b) = 0 \text{ or } J_t = J_b.$$
 (7)

Here, the fluxes are equal because there is no loss of molecules at the bottom and the flux into the feature equals the flux out of it. The flux ratio can be calculated using Eq. (5) as follows:<sup>1</sup>

$$\frac{J_b}{J_t} = \frac{k}{k+s-ks}. (8)$$

In Eq. (8), the flux at the bottom of the feature is a function of the reactive sticking coefficient s. For s = 1, the ratio of the two fluxes equals k, which is a function of aspect ratio. In the other extreme case of s = 0, the ratio of the two fluxes equals 1 and is independent on the aspect ratio. Figure 6 shows the values for  $J_b/J_t$ for a range of aspect ratios and sticking coefficients. The transmission coefficients are from Ref. 130 for cylinders. The case of s = 1can be approximated with the inverse of the depth.

The reactive sticking coefficient is determined by chemisorption. Chemisorption is suppressed at lower surface temperatures as illustrated in Fig. 3(b). Improved ARDE at lower temperatures can be explained by a reduced reactive sticking coefficient at lower temperatures. As the temperature is reduced further and physisorption 9 becomes an important adsorption mechanism, the sticking coefficient is reduced even further because the binding energies are

lower for physisorption vs chemisorption (see Table II).

At yet lower temperatures, the dependence should inverse because molecules stay physisorbed longer at lower temperatures.

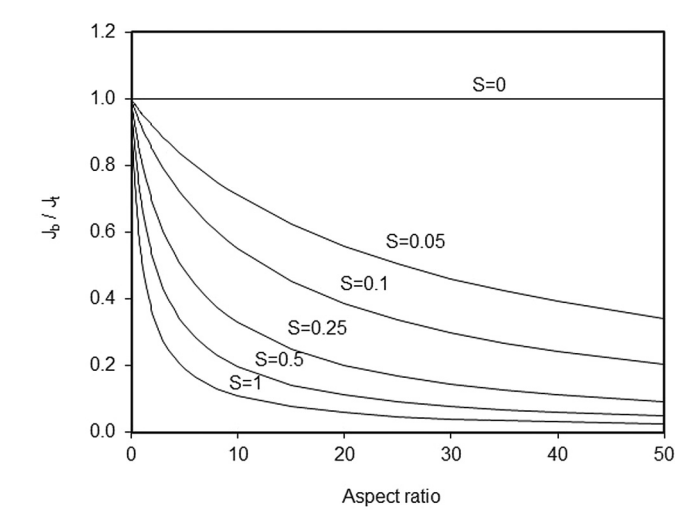


FIG. 6. Neutral fluxes at the bottom of a round cylinder normalized to the flux at the top based on Knudsen transport with a sticking coefficient s at the bottom of the cylinder.

Such an inversion may not be observed because physisorption opens the possibility for an additional transport mechanism: surface diffusion [Fig. 5(c)]. Surface diffusion plays a role, for instance, in technologies such a gas chromatography<sup>132,133</sup> and shale gas extraction<sup>134,135</sup> where gases are flowing through porous materials. Medved and Cerny published a review on surface diffusion in porous materials.<sup>133</sup>

If surface diffusion occurs during low temperatures etching, it should have a positive impact on ARDE. The total neutral flux at the bottom of a feature is, in this case, the sum of Knudsen flux and surface diffusion flux,

$$J_b = J_K + J_{diff}. (9)$$

Equation (9) is similar to Eq. (6) with the surface diffusion flux added. The reactive sticking coefficient on the sidewall is assumed to be 0 in the regime of dominant physisorption. The neutrals may get adsorbed or reflected at the etch front. Reflected neutrals will not travel back out of the feature in meaningful numbers due to surface concentration gradients. The existence of such a gradient means that the concentration at the etch front is low. This means the etch is in a neutral starved regime. Therefore, we assume that all neutrals are eventually consumed by an etch process at the etch front. The flux of etch products out of the feature does not interfere in the gas phase with the flux of reactants because of the low pressure. The total pressure of reactant and etch products is constant. Reaction products may also diffuse across the surface. This flux is in opposite direction to the surface diffusion flux of the reactants, and it is possible that these two surface fluxes interact. We ignore this possibility in this analysis.

The surface diffusion flux across a line of width a depends on the concentration gradient  $\Delta c/\Delta x$  and the diffusion coefficient  $D_s$  in  $\text{m}^2\text{s}^{-1},^{136}$ 

$$J_{diff} = -aD_s \, \frac{\Delta c}{\Delta x}.\tag{10}$$

In the case of surface diffusion in a round cylinder with diameter d, a equals the circumference of the cylinder:  $a = \pi d$ . The diffusion coefficient depends on the surface temperature T and an activation energy  $E_{a,diff}$ .

$$D_s = D_0 e^{-E_{a,diff}/k_b T}. (11)$$

Equations (2) and (11) imply that while the surface coverage with physisorbed molecules is larger, the molecules are less mobile

at lower surface temperatures. Figure 7 illustrates this schematically. Molecules with enough energy to overcome the diffusion barrier  $E_{a,diff}$  also have a higher probability to obtain enough energy to escape the surface to which they are bonded by  $E_{ads,phys}$ . However, in the case of etching high aspect ratio features, molecules that desorb are not lost. They adsorb on the opposite side of the feature.

Gilliland *et al.* proposed a simple correlation between the physisorption and diffusion energies, <sup>136</sup>

$$E_{a,diff} = \omega E_{ads.phys}.$$
 (12)

The coefficient  $\omega$  is called corrugation ratio. It is defined as the ratio of diffusion to physisorption energy and provides a measure of the modulation of the surface potential parallel to the surface. <sup>137</sup> A smaller corrugation ratio means molecules diffuse farther and is, therefore, desirable for the etching of high aspect ratio structures.

Combining Eqs. (4), (9), (10), (11), and (12), we obtain

$$J_n = c_K \Delta P/k_b N_A T + \pi dD_0 e^{-\omega E_{ads, phys}/k_b T} \frac{\Delta c}{\Delta x} . \tag{13}$$

Equation (13) details the constituents of the total flux to be the sum of the Knudsen and the surface diffusion fluxes. It is schematically illustrated in Fig. 8.

The neutrals enter the feature its top and physisorb on the sidewall. Before they desorb with random direction, they diffuse along the sidewall in the direction of lower concentration, which is down into the feature. When they desorb, they are not lost but adsorb on the opposite side of the feature where they continue to diffuse on the sidewall.

If the RIE process is neutral limited, the concentration at the  $\frac{\omega}{\omega}$  etch front is negligible and the average gradient  $\Delta c/\Delta x$  can be expressed as the concentration on the top of the feature divided by the depth of the feature l. The concentration can be expressed as surface coverage  $\theta$ . For a steady state surface coverage, the rate of adsorption and desorption is equal,

$$R_{ads} = R_{des}. (14)$$

The rate of desorption  $R_{des}$  is given in Eq. (2). Because we are discussing physisorption, we assume that the adsorption rates are independent on surface coverage. Atoms and molecules can adsorb on free or occupied surface site (see also Sec. II D). Under steady state conditions, the rate of adsorption  $R_{ads}$  can be expressed as the

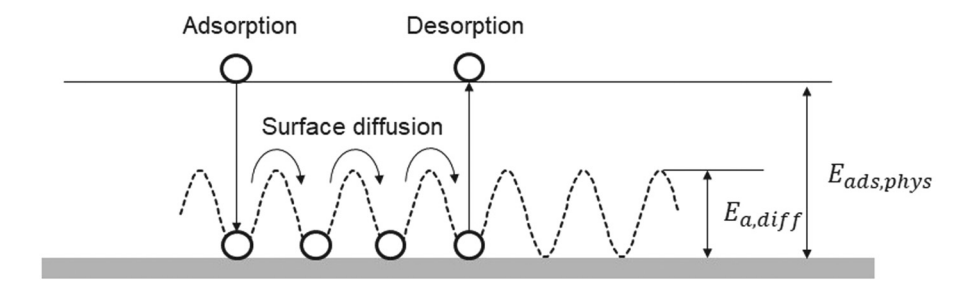


FIG. 7. Schematic illustration of the relationship between physisorption energies and activation energy for surface diffusion

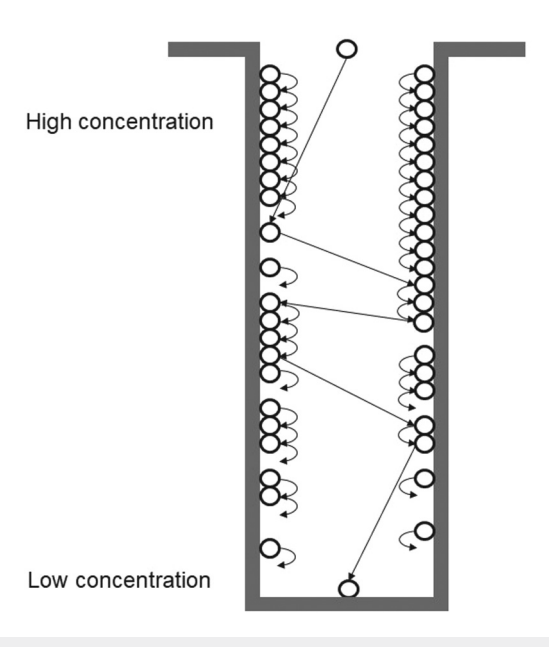


FIG. 8. Schematic illustration of synergistic Knudsen transport and surface diffusion

rate of arrival from the gas phase,

$$R_{ads} = \frac{P}{\sqrt{2\pi k_b mT}}. (15)$$

Equations (2), (14), and (15) yield

$$\theta = \frac{P}{k_0 \sqrt{2\pi k_b m T}} e^{E_{ads, phys}/k_b T}.$$
 (16)

The temperature in Eq. (2) is the surface temperature and that in Eq. (15) is the gas temperature. Here, we assume that the gas temperature rapidly becomes the surface temperature inside the etching feature due to interaction with the sidewall.

Using surface coverage to represent the concentration, we replace  $\Delta c$  in Eq. (13) with  $\theta$  from Eq. (16). We can also express  $\Delta x$ as the depth of the cylinder *l*,

$$J_n = P\left(\frac{c_K}{k_b N_A T} + \frac{\pi dD_0}{k_0 l \sqrt{2\pi k_b mT}} e^{(1-\omega)E_{ads,phys}/k_b T}\right). \tag{17}$$

The molecular flow conductance  $c_K$  for a round tube can be expressed as a function of the diameter d and length l of the tube and the gas velocity v,

$$c_K = \frac{\pi}{12} v \frac{d^3}{l}.$$
 (18)

The gas velocity is a function of temperature and mass. The mean of the magnitude of the velocity of the atoms or molecules in three dimensions can be expressed as

$$v = \sqrt{\frac{8k_bT}{\pi m}}. (19)$$

Insertion of Eqs. (18) and (19) into Eq. (17) gives

$$J_{n} = \frac{P}{l} \left( \frac{\pi d^{3}}{12 \ k_{b} N_{A} T} \sqrt{\frac{8k_{b} T}{\pi m}} + \frac{\sqrt{\pi} dD_{0}}{k_{0} \sqrt{2k_{b} m T}} e^{(1-\omega)E_{ads,phys}/k_{b} T} \right). \tag{20}$$

The flux of neutrals that arrives at the bottom of a feature is proportional to the gas pressure and inversely proportional to the depth. The flux is higher for smaller mass neutrals. The surface temperature dependence is complex. The Knudsen contribution decreases proportionally to the square root of the temperature. Because  $\omega$  is smaller than 1, the surface diffusion contribution increases exponentially and with the inverse of the square root of the temperature.

The Knudsen component scales with the cube of the diameter, while the surface diffusion component scales linearly. This means that the surface diffusion becomes more important for smaller diameters. Surface diffusion is, therefore, not only aspect ratio but also feature size dependent. Shallow and narrow features should see less ARDE compared to features with the same aspect ratio but larger dimensions. This effect can be used as a test for the presence of surface diffusion. Reduction in ARDE alone is not sufficient to identify the presence of surface diffusion because a diminishing o reactive sticking coefficient has a similar effect as shown in Fig. 6.

ive sticking coefficient has a similar effect as shown in Fig. 6. Equation (20) assumes the diffuse reflection of gas species off  $\frac{1}{8}$ the sidewall. When the sidewall is covered by physisorbed species, 8 the mass of the gas phase and physiorbed species is the same, binding energies are small, and the impact angle oblique due to shading effects. These are conditions under which specular reflection is possible. Specular reflection will increase the neutral flux to the bottom of the feature. This is true for pure Knudsen transport and for the conditions of slip flow, which can exist in MEMS etching applications. We assume in our analysis that the process is neutral limited and the concentration at the etch front is negligible. At very low temperatures and small ion fluxes, physisorbed species can cover the etch front completely and the concentration gradient is close to 0. In this case, ARDE is ion limited and determined by ion shading, which is a function of the width of the ion angular distribution and follows a different depth dependency. For intermediate cases, the attenuation of both the neutral and ion flux must be considered.

The ion flux to the sidewall changes the local surface coverage  $\theta$  and changes the concentration gradient which we assumed to be linear in Eq. (20). Gottscho et al. pointed out that the ion flux to the sidewall is subjected to ion shading. They proposed a modification of Eq. (8) taking into consideration the line-of-sight ion flux to the sidewall.<sup>84</sup> This requires knowledge of the ion angular distribution (IAD). Numerical solutions appear better suited to include ion scattering from the mask and the sidewall.

The effect of etch products is not considered in Eq. (20). These neutrals are transported out of the feature via Knudsen transport and surface diffusion. If the etching rates are high



enough, their diffusion across the surface may impact the surface diffusion of reactive neutrals in the opposite direction.

Let us now review surface diffusion properties of various gassurface systems. Table IV shows the results obtained by the laser induced thermal desorption of n-alkanes, <sup>137</sup> pentane isomers, <sup>138</sup> cycloalkanes, <sup>139</sup> tetramethyl silane, <sup>140</sup> and perfluoro-n-butane physisorbed on Ru(001). While these systems are not applicable to the high aspect ratio etching of semiconductor devices, interesting trends can be gleaned. Systems with larger desorption energies also have larger diffusion energies. The corrugation ratio for all hydrocarbon molecules in Table III is 0.30 within the measurement error. Substituting hydrogen with fluorine, however, reduces the corrugation ratio  $\omega$  from 0.29 (n-butane) to 0.21 (perfluoro-n-butane). The diffusion energy is smaller, and the desorption energy is larger for perfluoro-n-butane compared to n-butane. The smaller diffusion energy for perfluoro-n-butane is attributed to the larger van der Waals' radius for fluorine. A larger atom must average its physisorption interaction over a larger area on the surface because the atom is constrained to remain farther away from the surface. 141 The other trends from Table IV are

- 1.  $E_{a,diff}$  and  $E_{ads,phys}$  scale linearly with the ring size.
- 2.  $E_{a,diff}$  and  $E_{ads.phys}$  scale with the linear chain length.
- 3.  $E_{a,diff}$  and  $E_{ads,phys}$  scale inversely with the degree of branching.

If the results on Ru(001) can be generalized to other surfaces, smaller fluorinated molecules should be preferred for the low temperature etching of high aspect ratio features.

Tinck et al. calculated the rate of surface diffusion of physisorbed SiF<sub>x</sub> species by monitoring how far the species travel from the location where they first impact the surface. 99 Figure 9 depicts the results. The diffusion coefficients are considerably lower at 173 K compared to 300 K. Due to the less pronounced oscillations of atoms at cryogenic surface temperature, it is less likely for the physisorbed species to be pushed further along the surface. 99 In agreement with the experimental studies by Arena et al., they found that the surface diffusion coefficients decrease with the increasing size of the physisorbed species. In addition, they found a dependence of the degree of surface fluorination. More fluorine causes smaller surface diffusion coefficients. This effect, however,

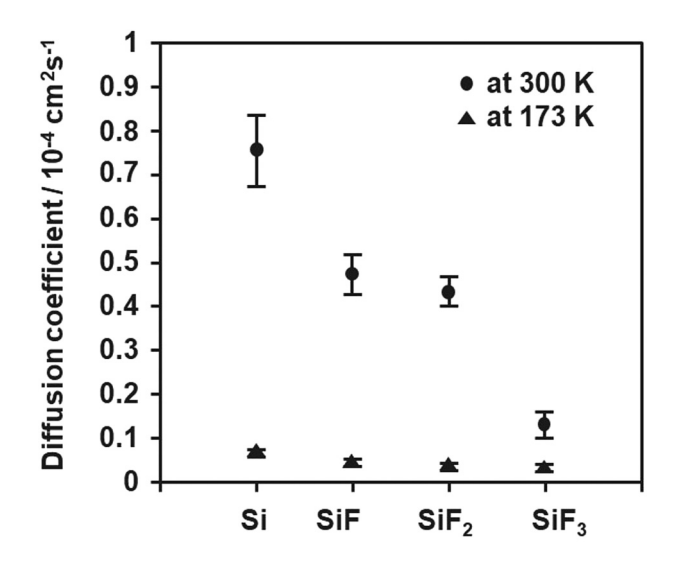


FIG. 9. Calculated diffusion coefficients for physisorbed SiF<sub>4</sub> on different SiF<sub>x</sub> surfaces for two different surface temperatures. Reprinted with permission from Tinck et al., J. Phys. Chem. C 118, 30315 (2014). Copyright 2014, American Chemical Society.

could be caused by a larger surface roughness of the fluorinated silicon surface rather than a chemical effect and may not be generalized.<sup>99</sup> When the authors compared the calculated surface diffusion coefficients with the desorption rates at 300 and 173 K, they found that the diffusion speed varies at maximum by one order of magnitude, while the difference in desorption rates differ by six  $\frac{3}{6}$  orders of magnitude. This means that under low temperature etch conditions, physisorbed species would likely find a site for chemisorption when diffusing across the surface before they find enough energy to desorb.<sup>99</sup> In other words, lower temperatures lead to less mobile molecules, but this effect is more than offset by the orders of magnitude lower rate of desorption.

Due to adsorbate-adsorbate interactions, the surface diffusion coefficient can be coverage dependent. 136,138,142 At low adsorbate

TABLE IV. Corrugation ratios for various organic molecules on Ru (001).

Molecule	Diffusion energy $E_{a,diff}/eV$	Desorption energy $E_{ads.phys}/eV$	Corrugation ratio $\omega$	Reference
Propane	0.13	0.47	0.27	137
Cyclopropane	0.09	0.34	0.25	139
n-Butane	0.15	0.51	0.29	137,140
Perfluoro-n-butane	0.12	0.59	0.21	139
n-Pentane	0.19	0.59	0.32	137,138
Isopentane	0.18	0.58	0.30	138
Neopentane	0.13	0.46	0.28	138
Cyclopentane	0.14, 0.14	0.51, 0.45	0.28, 0.32	138,139
n-Hexane	0.21	0.65	0.32	137
Cyclohexane	0.19	0.61	0.32	139
Tetramethylsilane	0.14	0.53	0.27	140

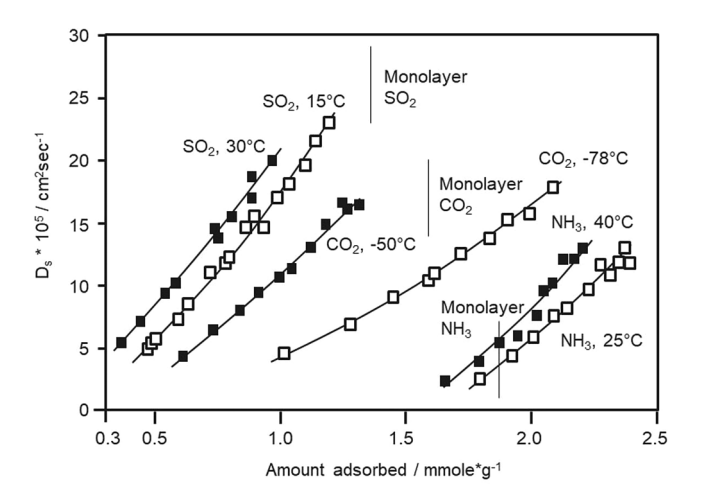


FIG. 10. Surface diffusivities of various gases on SiO2 as a function of coverage. Reprinted with permission from Gilliland et al., Ind. Eng. Chem. Fundam. 13, 95 (1974). Copyright 1974, American Chemical Society.

coverages, the activation energies are dominated by the adsorbatesurface interaction. As the adsorbate coverage is increased, adsorbate-adsorbate interactions may become important and can influence surface diffusion.<sup>83</sup> Coverage dependence of diffusion coefficients is a sensitive indicator for the adsorbate-adsorbate interaction. 91 Gilliland et al. reported increased diffusion coefficients when the surface coverage of SO2, CO2, and NH3 on SiO2 is increased as shown in Fig. 10.1

The surface diffusion coefficient of CO on Ru(100) in Fig. 11 also increases with coverage. 143 The data were modeled, assuming repulsive interaction between the CO molecules. An increase in the diffusion coefficient with coverage enhances the mass transport in high aspect ratio features further if high coverage or even multilayer coverage on the sidewall can be achieved.

In the case of repulsive adsorbate-adsorbate interaction, neutral transport via surface diffusion should be enhanced. These adsorbates can come from the etch gases, plasma dissociation, and aggregation products as well as etch products.

#### D. Process window

Table II states that physisorption can build up more than one layer of adsorbates, while chemisorption stops after the surface is covered. The dependence of physisorption coverage on pressure is described by the Brunauer-Emmett-Teller (BET) theory, 144 while chemisorption is described by the Langmuir theory. 145 The BET theory applies the Langmuir theory to each layer. The adsorption energy  $E_{ads,phys}$  for the first layer is larger than that for the subsequent layers. For additional layers,  $E_{ads,phys}$  is close to the enthalpy of liquefaction. The second and all following layers adsorb at higher pressures or lower temperatures than the first layer. Langmuir and BET isotherms are compared in Fig. 12.

For low pressures, the two curves are similar but as the pressure increases, the Langmuir curve saturates while the BET curve

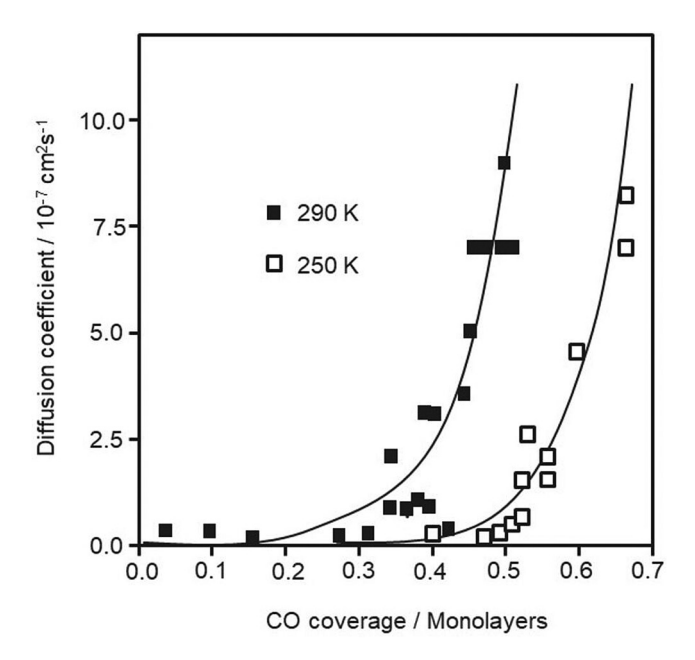


FIG. 11. Surface diffusion coefficients for CO on Ru(001) at 290 and 250 K vs CO coverage. Reprinted with permission from Deckert et al., J. Vac. Sci. Technol A 6 794 (1988). Copyright 1988, American Vacuum Society.

rises progressively with pressure. Figure 13 shows the experimental & results by Carman et al. for CF<sub>2</sub>Cl<sub>2</sub> on a carbon powder called \( \frac{1}{2} \) Carbolac. 129 While the curve for a temperature of 20 °C exhibits 8 Langmuir-like behavior, the curves for −21.5 and −33.1 °C represent typical BET curves. The isotherm at −33.1 °C reaches a near 🖁 vertical slope at pressures over 600 Torr. This is indicative of  $\vec{\omega}$ condensation.

While the isotherms in Figs. 12 and 13 provide important insights, the pressure range of etching processes is not a free parameter due to the requirements for plasma generation. The

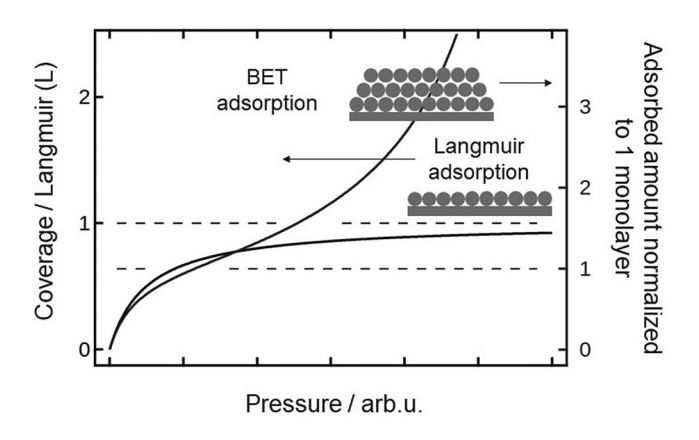
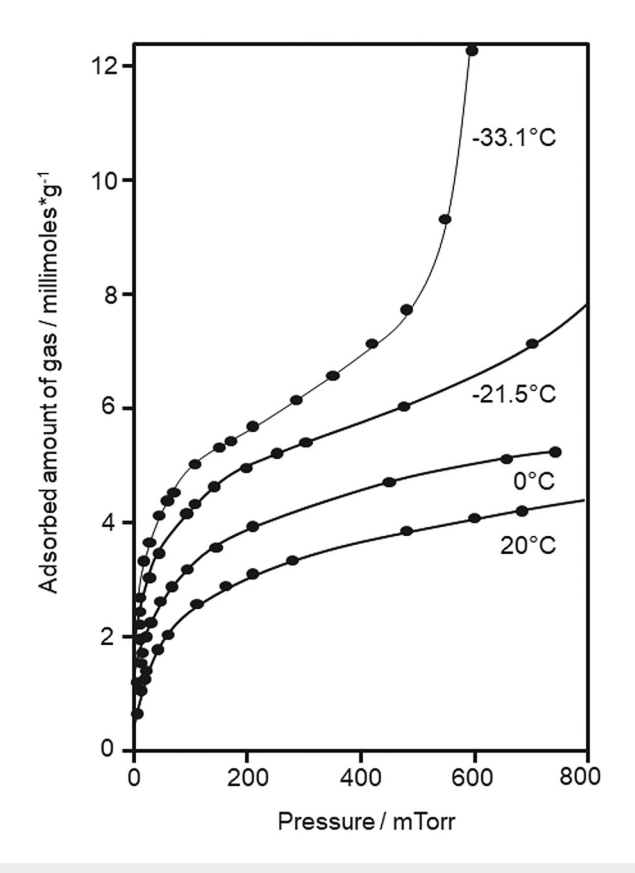


FIG. 12. Langmuir and multilayer adsorption isotherm as a function of pressure.





**FIG. 13.** Multilayer adsorption of  $CF_2CI_2$  on porous carbon powder. Reprinted with permission from P.C. Carman and F. A. Raal, Proc. R. Soc. Lond. A **209** 38 (1951). Copyright 1951, Royal Society of London.

wafer temperature, however, is independent in from the etch species generation, and hence, the isobars are more salient. Schematic isobars for chemisorption and physisorption are shown in Fig. 3. Considering the effects of multilayer physisorption and condensation, a schematic combined isobar is depicted in Fig. 14. As the temperature deceases, the surface coverage by chemisorbed species decreases because the activation barrier becomes too high. Molecules remain in the physisorbed state, and their surface coverage increases. At even lower temperatures, multilayer adsorption occurs. The slope of the coverage decrease is shown to be smaller to reflect smaller  $E_{ads.phys}$  for the second and subsequent layers. Finally, condensation triggers uncontrolled surface coverage. Figure 14 also shows the process windows for low temperature etching. The upper surface temperature limit for low temperature etching is a transition region where chemisorption is more important than physisorption. For plasma processes, chemisorption may extend to lower temperatures because of radical adsorption. The lower temperature limit of the process window is determined by condensation.

Next, we explore in more detail etching rates in a multilayer adsorption regime near the lower surface temperature limit. Figure 15 presents the evidence of higher rates of silicon at lower

temperatures with a high-density  $SF_6$  plasma at a pressure of 5 mTorr. <sup>4</sup> The etching rate peaks at -110 °C and drops at -150 °C, which is very close to the condensation temperature of  $SF_6$ .

Royer et al. conducted beam experiments in ultrahigh vacuum to explore the effects of multilayer adsorption on the etching of silicon with SF<sub>6</sub> gas and 500 eV neon ions. 107 They measured the amount of fluorine at the silicon surface after heating the sample back to room temperature. Because physisorbed SF<sub>6</sub> is desorbed at room temperature, the remaining fluorine concentration represents a mixed chemisorbed layer of silicon and fluorine. The silicon etch rate is assumed to be proportional to the fluorine concentration in this mixed surface layer. A higher fluorine concentration of this layer translates into a higher sputtering yield. The temperature dependence of the fluorine concentration in Fig. 16 demonstrates that the ion activated dissociative chemisorption of SF<sub>6</sub> molecules is furthered by the increase in the fraction of the surface sites occupied by physisorbed SF<sub>6</sub> molecules. <sup>107</sup> The fluorine concentration drops strongly at temperatures below 143 K or -130 °C, where ion activated dissociative chemisorption is strongly slowed down because the 500 eV neon ions do not reach the interface between the SF<sub>6</sub> adsorbate and the silicon substrate. <sup>10</sup>

Figure 17 shows that  $SF_6$  condenses at -158 °C for a pressure of 1 Pa or 7 mTorr. <sup>146</sup> Therefore, the low temperature drop in the etching rate in Tsujimoto's experiments can be attributed to the onset of condensation. The pressure in the beam experiment by Royer *et al.* was three orders of magnitude lower than for Tsujimoto *et al.*; hence, condensation can be ruled out in Royer's experiment. Rather, a multilayer film with a thickness of a few nanometers was enough to shield the silicon surface from the 500 eV neon ions.

The activation conditions such as ion flux, ion energy, and presence of photons and electrons must also be considered when comparing the beam experiments by Royer *et al.*<sup>107</sup> with the direct plasma data by Tsujimoto *et al.*<sup>4</sup> Ions with higher energies should penetrate a thicker layer of physisorbed SF<sub>6</sub>. Even though the ion energy is higher in the beam studies than in the plasma experiments (500 vs about 40 eV), etching stops at higher temperatures. It is possible that a higher ion flux or the effect of photons and electrons from the plasma reduced the thickness of the adsorbed layer.

The ability to use plasma exposure to enable etching below the  $SF_6$  condensation temperature has been demonstrated by Bestwick *et al.* in a reactor with one electrode powered by 13.56 MHz.<sup>8</sup> They cooled the RF electrode with liquid nitrogen such that the sample surface reached a temperature of  $-160\,^{\circ}\text{C}$ . The oscillations in the interferometer signal in Fig. 18 are the result of  $SF_6$  condensing on the sample surface. When the plasma is ignited,  $SF_6$  desorbs, and silicon etches. Compared to the room temperature experiments, the etching rate was higher at low temperatures for RF powers above 700 W.

Chevolleau *et al.* studied the effect of ion energy and current density for the low temperature etching of silicon with  $SF_6$  in detail. <sup>19</sup> They found that at low wafer temperature, the surface coverage with fluorine containing molecules is a result of a delicate balance between the adsorption and desorption rates. Temperature, ion flux, and ion energy must be balanced to maximize the etching yield and rate. <sup>19</sup>

Physisorption		Chemisorption
Multilayer	Partial Monolayer	
Low tempera	ture Etching	Conventional Etching
	3 3 3 3 3 3 3 3 3 3 3 3 3 3 3 3 3 3 3	
,	proturo / orb. u	
	Multilayer  Low tempera	Low temperature Etching

FIG. 14. Process window for low temperature etching.

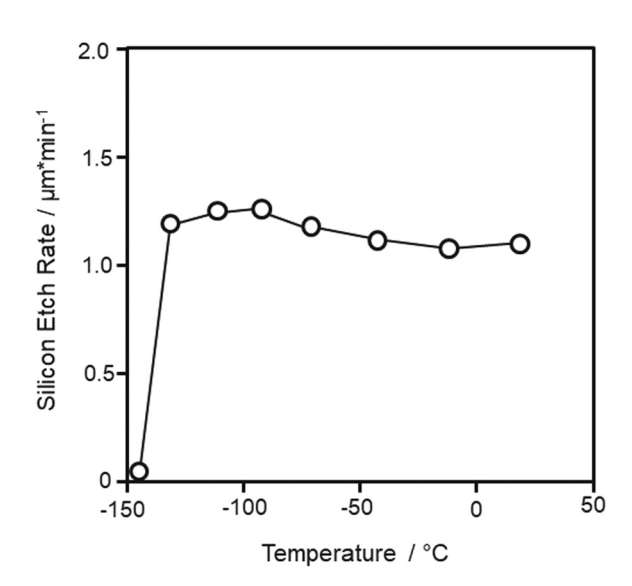


FIG. 15. Temperature dependence of the etching rate of silicon in a SF<sub>6</sub> plasma. Reprinted with permission from Tsujimoto et al., Jpn. J. Appl. Phys. 30, 3319 (1991). Copyright 1991, IOP Publishing Ltd.

The type of fluorine gas is obviously important in determining lower temperature limit. Mullins, and Coburn demonstrated the lower temperature limit. Mullins and Coburn demonstrated increasing etching rates for temperatures as low as -196 °C in a beam experiment with fluorine atoms and 1 keV argon ions. 147

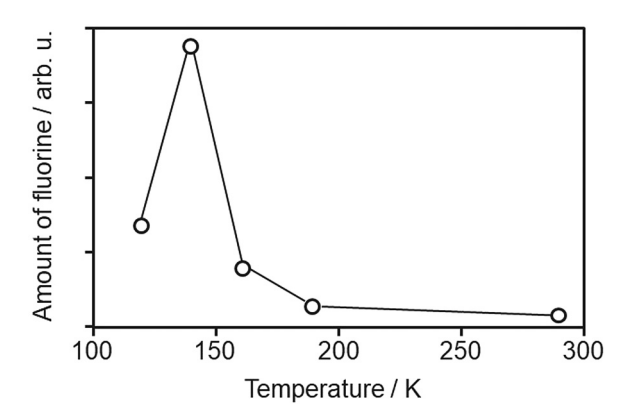


FIG. 16. Fluorine concentration at the surface of silicon after simultaneous exposure a neon ion beam and  ${\rm SF}_6$  background gas as a function of temperature. Reprinted with permission from Royer et al., J. Vac. Sci. Technol. A 14, 234 (1996). Copyright 1996, American Vacuum Society.

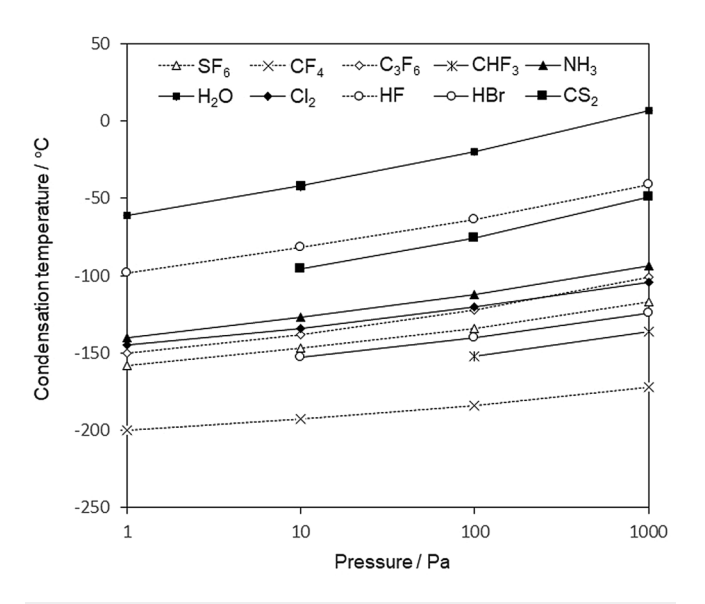
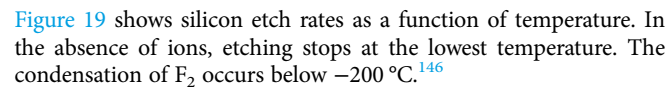


FIG. 17. Condensation temperatures of gases relevant for semiconductor etching. Values from Ref. 146



Besides implications for etching rates, operating in a multilayer physisorption regime should produce better ARDE performance. If the sidewall is covered with more than one physisorbed layer, diffusion would be further enhanced because  $E_{a,diff}$  is lower for the second and subsequent layers. <sup>148</sup> Capillary condensation, in at least the initial stages, produces a rapid rise in surface diffusion coefficients. 129 Horiguchi et al. even hypothesized that for physisorbed multilayers, a hydrodynamic model maybe better suited to describe mass transport.14

While plasma stimulated desorption can extend the theoretical process window toward lower wafer temperatures, the effect of capillary condensation can push it toward higher temperatures for

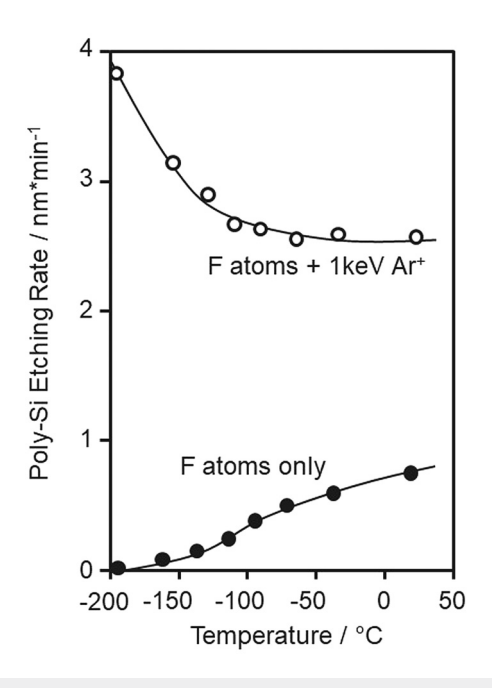


FIG. 19. Silicon etch rates as a function of temperature during exposure to F atoms with and without 1 keV argon ion bombardment. Reprinted with permission from C. B. Mullins and J. W. Coburn, J. Appl. Phys. 76, 7562 (1994). Copyright 1994, AIP Publishing LLC.

small features. Capillary condensation is a phenomenon whereby a gas condenses to a liquid-like phase in a pore at a pressure P less than the saturation pressure of the liquid  $P_0$ . The effect is described by the following Kelvin equation:  $\frac{150}{6}$ 

$$\ln \frac{P}{P_0} = -\frac{2\gamma V_m}{rRT},$$
(21)

where  $\gamma$  is the surface tension,  $V_m$  is the molar volume of the liquid, r is the radius of the droplet at the liquid-vapor phase

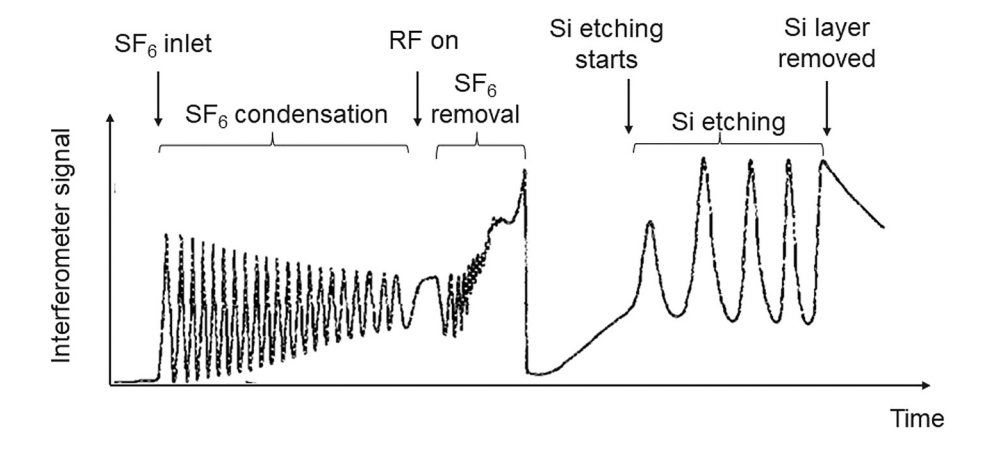


FIG. 18. Laser interferometer signal during a low temperature etching of silicon with SF<sub>6</sub>. Reprinted with permission from Bestwick et al., Appl. Phys. Lett. 57, 431 (1990). Copyright 1990, AIP Publishing LLC.



boundary, R is the universal gas constant, and T is the surface temperature. Fisher et al. demonstrated experimentally that this equation is valid for organic liquids with meniscus radii as small as  $4 \,\mathrm{nm}^{151}$  and for water as small as  $9 \,\mathrm{nm}^{152}$  For a circular hole, r is the radius of the meniscus of the condensed liquid, which is equal to the radius of the circular hole less the thickness of the adsorbed film on the sidewall. Figure 20 illustrates the effect for hydrofluoric acid at -60 and -100 °C. HF is characterized by strong polarity and, therefore, condenses at relatively high temperatures (see Fig. 17). The molecular volume at these temperatures is calculated using density data from Simons and Bouknight. Figure 20 shows that the pressure at which HF condenses drops precipitously for hole radii below 40 nm. Typical radii for holes used to manufacture 3D NAND memories are between 45 and 55 nm. HF is not widely used as an etch gas but is formed in the plasma by the recombination of fluorine and hydrogen atoms, produced by the plasma dissociation of parent gases. The concentration should be at least one order of magnitude below the pressure of the feed gases, which is around 10 mTorr. We estimate that the condensation of HF could play a role for radii smaller than 10 nm at −60 °C and below 20 nm at -100 °C. Such small radii can be present at the etch front, which can be narrow. Capillary condensation in very narrow etch fronts would result on a more squared etch front. Because capillary condensation is a function of the radius and not the aspect ratio, it must be considered in logic etch application where the aspect ratios are more relaxed compared to 3D memory structures, but the dimensions are in the range of a few nanometers. Rough sidewalls can be viewed as very small features with dimensions in the range of a few nanometers and below. If these features with filled with liquids, sidewall roughness can be improved.

The dipole moment of water is 1.85 D (Ref. 154) and 1.91 D for HF.  $^{155}$  On flat surfaces, water condenses at similar temperatures as HF (see Fig. 17). Water is a constituent of the background gas, and condensation can limit the lowest temperature possible for etching.  $^{67}$  Due to capillary effects, H<sub>2</sub>O condensation would occur at the smallest features first. The effect is not reproducible because

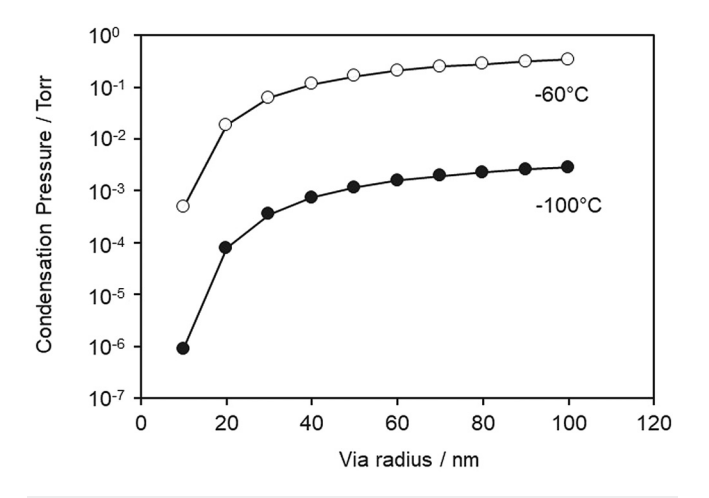


FIG. 20. Calculated pressure for the capillary condensation of hydrofluoric acid.

different etch chambers have different background moisture contents. To avoid wafer to wafer and chamber to chamber repeatability issues, etch gases must be selected such that physisorption occurs at higher pressures. Alternatively, low temperature etching may require hardware, which provides a lower background pressure if temperatures below  $-100\,^{\circ}\mathrm{C}$  are to be used.

# E. Sidewall passivation

Sidewall passivation is essential for achieving vertical profiles. Possible passivation mechanisms in low temperature etching include the adsorption of precursor gases and etching products on the sidewall as well as diminishing reaction rates at low substrate temperature. 103 Coburn mentioned low temperatures as one of the approaches to reduce etching in the lateral direction. <sup>156</sup> Tachi et al. reported temperatures to achieve vertical profiles for a wide range of materials and etch gases.<sup>3</sup> The same group showed that silicon profiles etched with SF<sub>6</sub> and NF<sub>3</sub> plasma changed from being undercut to vertical when the temperature was lowered below −100 °C.<sup>2,4</sup> The condensation temperature of SiF<sub>4</sub> is about −166 °C at the pressure of the experiment (6.7 mTorr), but sidewall etching stopped at -144 °C. They concluded that vertical profiles must, therefore, be the result of a lower spontaneous etching rate. Bartha et al. were able to reproduce these results only by adding oxygen to the mix.<sup>17</sup> They argued that the use of a quartz window in the work of the Japanese group was a source of oxygen, and the sidewall passivation mechanism was the condensation of SiO<sub>x</sub>F<sub>y</sub>, for instance SiOF<sub>3</sub>.<sup>27</sup> The condensation temperature for silicon oxyfluorides is higher than that for  $SiF_4$ . The boiling point of  $Si_2OF_6$  is −23 °C at atmosphere pressure.

Another approach to generate condensing species for silicon sidewall passivation is to use chlorine. At 7 Torr, the condensation temperatures for SiCl<sub>4</sub> or SiF<sub>4</sub> are -39 or -132 °C, respectively. Also, passivation with fluorocarbon polymers is widely used in the etching of silicon oxides and nitrides. Tachi *et al.* studied C<sub>x</sub>F<sub>y</sub> deposition from a CHF<sub>3</sub> plasma and found a threefold increase in the deposition rate when the wafer temperature was decreased from room temperature to -110 °C. This type of passivation mechanism can create too much polymer especially on the top of the features. Generally, low temperature processes use less passivation compared to conventional processes, which contributes to higher etching

In Secs. III and IV, we review low temperature etching for specific applications with focus on the performance benefits based on the mechanisms reviewed so far.

# III. APPLICATIONS

#### A. High aspect ratio silicon etching

A review of deep silicon etching can be found in a paper by Wu *et al.*<sup>159</sup> Dussart *et al.* summarized the development of deep silicon etching at low wafer temperatures.<sup>31</sup> One of the first reports on low temperature etching by Tachi *et al.* was devoted to the patterning of silicon with  $SF_6$ .<sup>2</sup> Figure 21 shows an increase in the silicon etching rate, higher selectivity, and less undercut profile as the temperature was decreased. Subsequently, low temperature etching was continuously improved over the next 20 years as one of

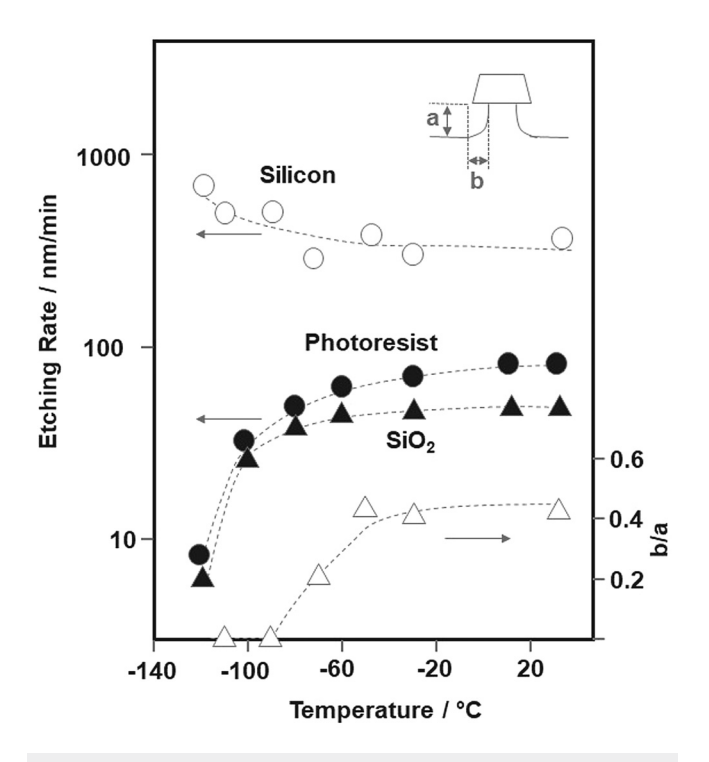


FIG. 21. Temperature dependence of the etching rate of silicon in a SF<sub>6</sub> plasma. Reprinted with permission from Tachi et al., Appl. Phys. Lett. 52, 616 (1988). Copyright 1988, AIP Publishing LLC.

the deep silicon etch technologies. Today, it has been largely replaced by a room temperature process, which utilizes cycling between C<sub>4</sub>F<sub>8</sub> polymer deposition and SF<sub>6</sub> etching. <sup>159</sup> A comparison between low temperature etching and high temperature cyclic processing can be found in the work by Walker. 160 The combination of cyclic processing with lower temperatures is another interesting approach. Tachi *et al.* reported decreasing etching rates for photoresist and SiO<sub>2</sub> masks as the temperature is reduced while the etching rate for silicon is increasing.2 This results in a higher selectivity, which is extremely desirable for high aspect ratio etching. A selectivity of up to 1000 has been reported for SiO2 and over 100:1 for photoresist. 160 The selectivity values for the cyclic process are 200:1 for SiO<sub>2</sub> and 75:1 for photoresist.<sup>1</sup>

High aspect ratio silicon etching is a vehicle to test whether ARDE is reduced under low temperature conditions as predicted by the mechanisms described in Sec. II. Blauw et al. reported greatly reduced ARDE for a low temperature deep silicon etch with SF<sub>6</sub> and 12% O<sub>2</sub> at a temperature of -105 °C, a pressure of 2 mTorr, and a bias voltage of -12 V. This temperature was low enough for SF<sub>6</sub> to physisorb even at very low pressure. The results are shown in Fig. 22. Under conditions of low temperature, low pressure, and low ion energies, the etch depth is a linear function of time and trenches with 290 nm width at the top of the feature etch to 90% depth vs 2080 nm wide trenches. The largest aspect ratio is 55:1.

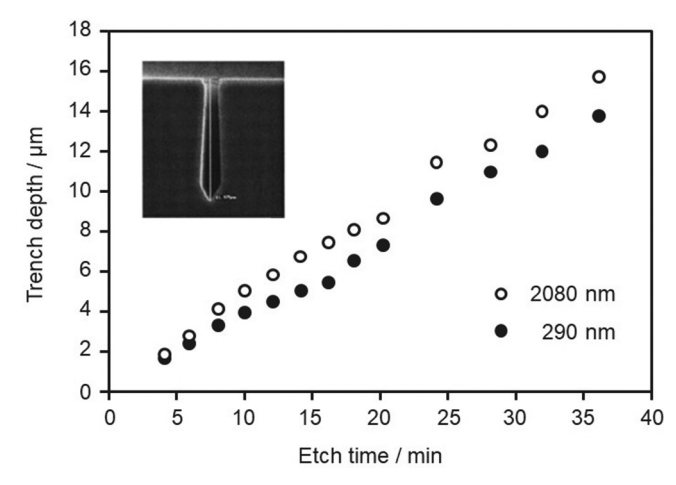


FIG. 22. Etch depth as a function of time for low temperature silicon trench etching. The trenches were etched in a high-density plasma with a wafer temperature of -105 °C. The SF<sub>6</sub> flow was 22.5 SCCM, the O<sub>2</sub> flow was 3.3 SCCM, and the pressure was 0.30 Pa. Reprinted with permission from Blauw et al., J. Vac. Sci. Technol. B 18, 3453 (2000). Copyright 2000, American Vacuum Society.

The authors reported that ARDE emerged when the ion energy and flux or temperature were increased. They also found that under low temperature conditions, 1000 surface atoms are 2 removed per impinging ion. This is an extremely large value and E two to three orders of magnitude higher than for room temperature RIE. It could be explained by evoking physisorption of etch gases 8 and thermal desorption of loosely bonded SiF<sub>x</sub> reaction products.

Walker reported that the etching rate of a low temperature  $\frac{1}{2}$ deep silicon process is reduced by 50% for trenches with an aspect  $\frac{1}{\omega}$ ratio of 35:1. In the same report, data for a room temperature cyclic etching of holes are shown. The etching rate is reduced by 85% for an aspect ratio of 35:1. 160 These values cannot be compared directly with the data in Fig. 23 because trenches have lower ARDE than cylinders due to the geometry for ion shading.

The inset in Fig. 22 shows that under the condition of aspect ratio independent etching, the bottom of the profile facetted in the (111) direction of silicon. This effect is called crystal orientation dependent etching (CODE) and was reported first by Wells et al. and later by Dussart et al. 18,31 Zijlstra et al. reported that the Si (100)/Si(111) etch rate ratio increases when decreasing the temperature. A maximum is reached at around -80 °C.<sup>23</sup> CODE follows the same process trends as low ARDE etching. 12 In summary, there is some indication that physisorption and surface diffusion could be present in low temperature silicon etching, but more work is needed to establish the importance of these effects.

# B. High aspect ratio dielectric etching

Attempts to etch silicon oxide under low surface temperature conditions were made in the late 1980s. Ohiwa et al. studied the temperature effect in the etching of  $1 \mu m$  silicon oxide cylinders with a CHF<sub>3</sub> plasma. Figure 23 shows that the etching rate

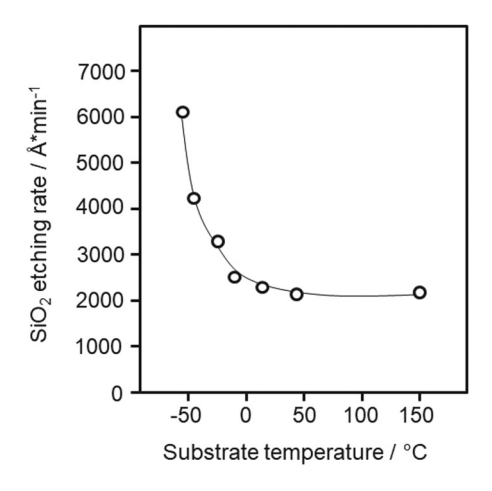


FIG. 23.  $SiO_2$  etch rate in a CHF $_3$  plasma as a function of wafer temperature. Reproduced with permission from Ohiwa *et al.*, Jpn. J. Appl. Phys. **31**, 405 (1992). Copyright 1992, IOP Publishing Ltd.

strongly increased for temperatures below 50 °C. The deposition rate of reactive fluorocarbon polymers on silicon also increased up to a temperature of -50 °C as shown in Fig. 24. The strong decrease of the deposition rate below -50 °C was attributed to the lack of chemical bonding between the adsorbed species. Some of the film may also have been desorbed when the wafer was heated up to measure the film thickness. 101 Ohiwa et al. explained the finding that the etch rate increased, while the passivating polymer film thickness also increased with a higher fluorine content in the low temperature fluorocarbon films. 101 Despite a higher reactivity of the polymer film, the profiles became more tapered at low tempera-Tachi et al also reported an increase in the polymer deposition rate for CHF<sub>3</sub> plasma for temperature as low as -100 °C.<sup>3</sup> The authors consider physisorption as the key factor to this deposition rate increase on the cooled surface.

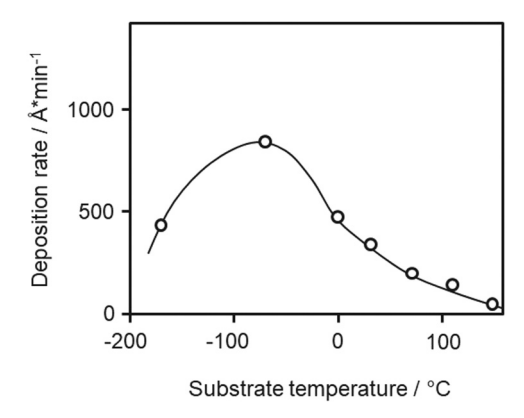


FIG. 24. Polymer deposition rate in a CHF3 plasma as a function of wafer temperature. Reproduced with permission from Ohiwa et al., Jpn. J. Appl. Phys. 31, 405 (1992). Copyright 1992, IOP Publishing Ltd.

These early results indicated the potential of low surface temperatures for increasing etching rates but also the challenge of polymer control for C<sub>x</sub>H<sub>v</sub>F<sub>z</sub> based chemistries. Polymer control becomes a critical challenge in high aspect ratio dielectric etching where polymers on the top of the feature shrink the cross section of the opening and thereby reduce the ion flux to the bottom of the feature, which slows the etching rate. Polymers on the top of the feature also become facetted from ion sputtering, which causes ion deflection and profile bowing.<sup>164</sup> The etching mechanism for SiO<sub>2</sub> with hydrofluorocarbon gases such as CF<sub>4</sub>, CHF<sub>3</sub>, CH<sub>2</sub>F<sub>2</sub>, C<sub>4</sub>F<sub>6</sub>, and C<sub>4</sub>F<sub>8</sub> relies on the deposition of reactive polymers. Mass transport via surface diffusion is hindered by the size of some of these molecules and the fact that they can react with each other on the surface to form even larger molecules. Therefore, different etch chemistries must be considered for low temperature dielectric etching.

Iwase et al. investigated the temperature dependence of dielectric etching with a mixture of HBr, a fluorocarbon gas and The flows of HBr and the unnamed fluorocarbon gas were nearly equal. The large amount of hydrogen from HBr made the plasma less polymerizing or "leaner." The important target application for this process is the patterning of high aspect ratio holes for the formation of vertically stacked flash memory cells. They are produced in two different integration schemes based on multilayer stacks of silicon oxide and poly-Si (OPOP) and stacks of silicon oxide and silicon nitride (ONON) into which high aspect ratio holes were etched using a carbon mask. Figure 25 shows that the etching rates 101 an uncommend of to 20 °C, which increased when the temperature is decreased from 60 to 20 °C, which is unchanged. 165 % shows that the etching rates for all the silicon containing films o Higher etching rates, more vertical profiles, and a flat etch front 8 were demonstrated on patterned OPOP (Ref. 168) and ONON wafers.16

Figure 26 shows the example of ONON structures. 165 The underlying passivation mechanism for both OPOP and ONON is based on NH<sub>4</sub>Br, which is formed in increasing quantities as the temperature is decreased. The authors supported this claim with

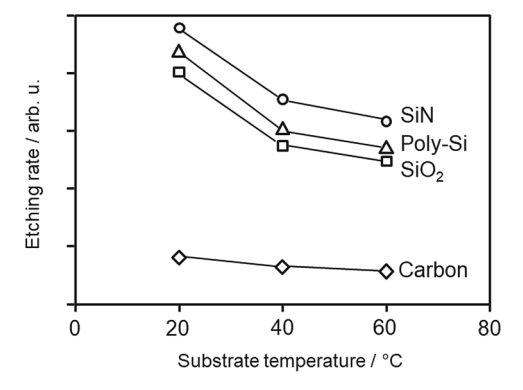


FIG. 25. Blanket wafer etching rate of SiO<sub>2</sub>, SiN, poly-Si, and carbon as a function of wafer temperature. Reproduced with permission from Iwase et al., Jpn. J. Appl. Phys. 57, 06JC03 (2018). Copyright 2018, IOP Publishing Ltd.



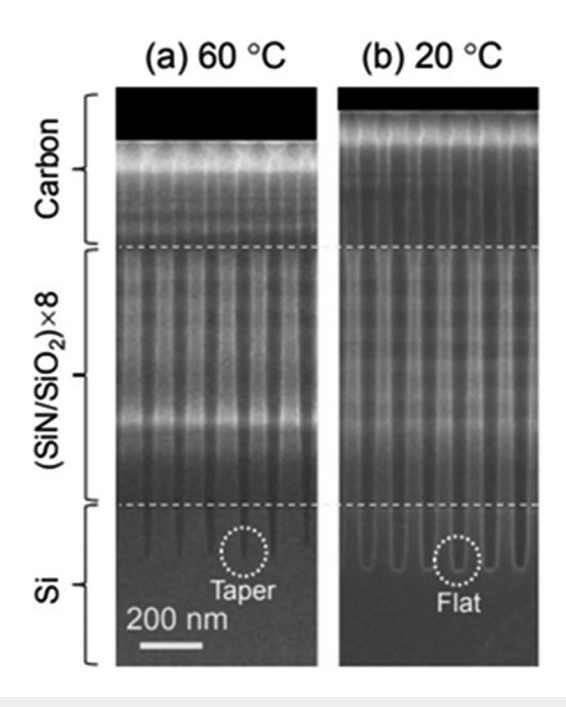


FIG. 26. Cross-sectional SEM images of 50-nm-diameter holes in a SiN/SiO<sub>2</sub> stacked layer. Substrate temperatures were (a) 60 and (b) 20 °C. Etch time was adjusted to obtain uniform hole depth. Reproduced with permission from Iwase et al., Jpn. J. Appl. Phys. 57, 06JC03 (2018). Copyright 2018, IOP Publishing

thermodynamics calculations, 168 thermal desorption spectroscopy,<sup>167</sup> imaging secondary neutral mass spectrometry,<sup>167</sup> mass spectroscopy. 165 At 20 °C, the authors found a fluorocarbon polymer layer with (NH<sub>4</sub>)Br<sub>2</sub> inclusions. 167 The increase in the poly-Si etching rate at low temperatures is possibly caused by the volatilization of silicon and carbon with increased amounts of N, H, and Br, 167 while a thicker and less hydrofluorocarbon containing layer may assist the etching of SiO<sub>2</sub> and SiN. A uniform top to bottom distribution of bromine was found in the sidewall passivation layers of the ONON structures. 165 The authors proposed a mechanism where highly mobile N<sub>2</sub> and HBr and their fragments adsorbed at the surface, traveled to the bottom of the feature, and synthesized NH<sub>4</sub>Br at the etch front. Whether the transport was aided by surface diffusion cannot be answered from the studies. Regardless, the authors found greatly reduced ARDE for ONON at low temperatures as illustrated in Fig. 27.16

The formation of compounds such as ammonium bromide is a key technology for one-step etching of holes in OPOP and ONON stacked films. 165 Another compound that can be synthesized on the surface of these films in the presence of hydrogen, fluorine, and nitrogen is ammonium fluorosilicate (NH<sub>4</sub>)<sub>2</sub>SiF<sub>6</sub>. The ability to etch SiO<sub>2</sub> has been demonstrated in downstream plasmas with NH<sub>3</sub> and NF<sub>3</sub> (Ref. 169) or NF<sub>3</sub> and H<sub>2</sub> (Refs. 170 and 171) as well as thermally activated mixtures of NH<sub>3</sub> and NF<sub>3</sub>. The combinations of fluorine, nitrogen, and hydrogen containing gases produce hydrogen fluoride at the surface to form (NH<sub>4</sub>)<sub>2</sub>SiF<sub>6</sub>,

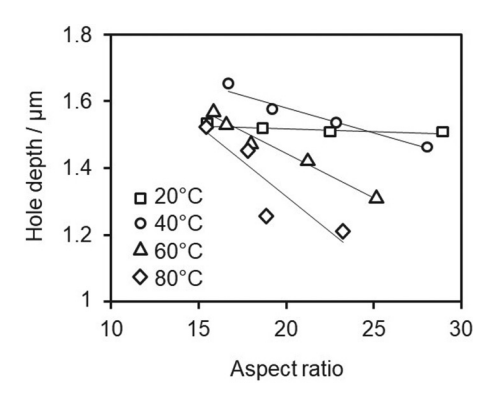


FIG. 27. Dependence of ONON hole depth, defined as (etch depth + mask height), on the aspect ratio for different wafer temperatures. Reproduced with permission from Iwase et al., Jpn. J. Appl. Phys. 57 06JC03 (2018). Copyright 2018, IOP Publishing Ltd.

through the reaction of silicon oxide with  $NH_4F$  or  $(NH_3 + HF)$ . <sup>171</sup> In the case of SiN, the nitrogen is part of the film and gases containing just hydrogen and fluorine such as CHF3 can be used for radical etching.<sup>62</sup> The formation of (NH<sub>4</sub>)<sub>2</sub>SiF<sub>6</sub> on SiO<sub>2</sub> is selflimiting at low temperatures<sup>62,171</sup> but not on SiN.<sup>171</sup> Etching of SiN selectively to SiO2 using a downstream plasma of chlorine trifluoride ClF<sub>3</sub> and H<sub>2</sub> has also been reported.

Ammonium fluorosilicate decomposes at temperatures above \$\frac{1}{2}\$ 100 °C, forming NH<sub>3</sub>, SiF<sub>4</sub>, and HF. It also evaporates when \$\frac{1}{2}\$ exposed to ions, electrons, or photons. The formation of (NH<sub>4</sub>)<sub>2</sub>SiF<sub>6</sub> consumes silicon compounds at the surface and provides self-limiting sidewall passivation at the same time. Ion bombardment at the etch front removes the passivation and enables and enables directional etching. At low surface temperatures, the feed gases can physisorb at the surface and travel to the etch front via Knudsen transport or a combination of surface diffusion and Knudsen transport. The precursor gases can be selected considering their condensation temperatures,  $E_{a,diff}$ , and  $E_{ads.phys}$ , to optimize surface coverage and transport inside the high aspect ratio features. This is a fundamentally different etching mechanism than conventional fluorocarbon-based etching. 174 Higher etching rates and reduced ARDE are observed for this class of low temperature dielectric etching. Figure 28 depicts the depth dependent etching rates of a multilayer SiO<sub>2</sub>/SiN stack with 3200 nm carbon hardmask using a conventional etching process with C<sub>4</sub>F<sub>8</sub>, C<sub>4</sub>F<sub>6</sub>, and argon above room temperature and a pressure around 20 mTorr. The plasma is generated in a dual frequency capacitively coupled reactor. Figure 28 also shows the etch rates for a process operating at -20° C at a comparable pressure but using a carbon free fluorine gas instated of C<sub>4</sub>F<sub>8</sub> and C<sub>4</sub>F<sub>6</sub>. The low temperature process exhibits meaningfully lower etch rate reduction with depth compared to the conventional process. The etching rate at depths shallower than 3000 nm is higher for the conventional process in this specific set of experiments. While the etching rates at shallower depth can be tuned for processes, the reduced sensitivity of the low temperature process is generally observed.



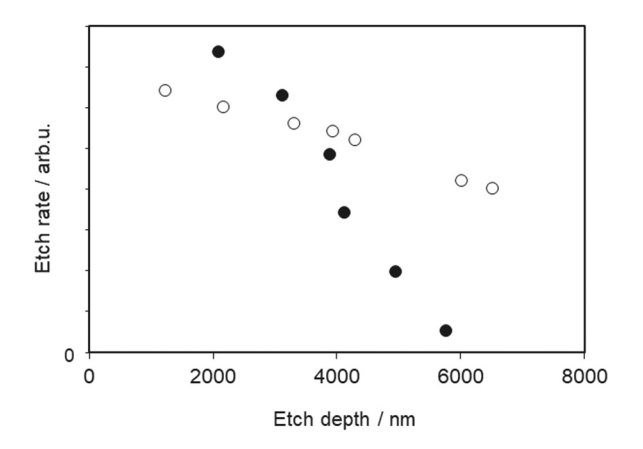


FIG. 28. Etch rate vs depth for a conventional (solid circles) and low temperature etching processes (open circles) of circular holes with a diameter of

#### C. Atomic layer etching

Physisorption can be used to deliver reactive species to a surface as part of a directional ALE process. Directional ALE is a cyclic process where the surface bonds are chemically weakened in a first step, and the resulting modified layer is removed by the impact of directional species such as ions or fast neutrals. <sup>175</sup> One of the first demonstrations of this etching method utilized surface temperatures as low as -60 and -160 °C to etch silicon. The surface was modified by species from a CF<sub>4</sub>/O<sub>2</sub> downstream plasma, and the limiting step was the accumulation of fluorocarbon polymers.<sup>177</sup> Experiments with downstream NF<sub>3</sub> and 5% F<sub>2</sub> in helium also resulted in measurable material removal per cycle. The authors demonstrated experimentally that the physisorption of fluorine molecules at the surface and ion bombardment induced chemical reactions are responsible for etching. Etching of silicon lines and spaces resulted in ARDE-free profiles when the argon ion removal step was saturated as shown in Fig. 29.

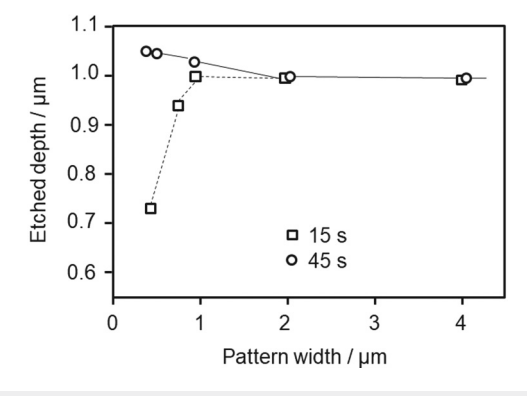


FIG. 29. Etch depth vs pattern width for a low temperature ALE process with saturated (45 s) and undersaturated argon ion removal step (15 s). Reproduced with permission from Sakaue et al., Jpn. J. Appl. Phys. 29, 2648 (1990). Copyright 1990, IOP Publishing Ltd.

Ohiwa et al. conducted ALE experiments where they deposited fluorocarbon polymers at −70 °C onto SiO<sub>2</sub> using a CHF<sub>3</sub> plasma and argon plasma to stimulate etching.<sup>101</sup> They found higher etching rates of SiO2 when a 10 nm thin fluorocarbon layer was present compared to a pristine SiO2 surface. The benefit of low wafer temperature operation in this example is a higher fluorine concentration in the polymer film. The ion energy in these experiments was not reported. Shinoda et al. applied the idea of modifying the surface with a hydrofluorocarbon-based downstream plasma modification at -20 °C to the etching of tungsten. 61 The removal of tungsten fluoride was accomplished by rapid thermal annealing of the sample. Conformal etching of tungsten was demonstrated. Dallorto et al. reported on the ALE of SiO<sub>2</sub> with a CHF<sub>3</sub> plasma modification and an argon ion removal step for temperatures between -40 and 20 °C. 64,65 While the temperature sensitivity is not very pronounced, they obtain the best process results for a wafer temperature of -10 °C.

Kim et al. reported on SiN etching using CH<sub>3</sub>F gas adsorption without plasma at 80 °C and argon ion bombardment. 102 XPS analysis revealed the presence of a surface modification layer after CH<sub>3</sub>F gas exposure, which contained various forms of SiF<sub>x</sub> and Si (CH<sub>3</sub>)<sub>x</sub>, as well as nitrogen bonded to carbon. The authors concluded that this reactive layer is formed during the chemisorption of CH<sub>3</sub>F. Sridhar et al. also conducted SiN ALE experiments at 80 °C with CF<sub>4</sub>, CHF<sub>3</sub>, CH<sub>2</sub>F<sub>2</sub>, and CH<sub>3</sub>F gas adsorption and argon ion bombardment.<sup>66</sup> When the argon gas stabilization time after the evacuation of the  $CH_xF_{4-x}$  and before striking plasma was extended, the amount of material etched per cycle (EPC) decreased o as shown in Fig. 30. This can be explained by the argon atom collision induced desorption of  $CH_xF_{4-x}$  molecules. Based on this  $\frac{7}{8}$ observation, the authors concluded that the CH<sub>x</sub>F<sub>4-x</sub> molecules 8 were physisorbed at the surface. The results of these experiments indicate that the physisorption of precursors is sufficient to cover the surface, allowing etching in the subsequent plasma assisted activation and desorption step.

Antoun et al. performed ALE on SiO2 samples cooled down below -100 °C. 63,67 C<sub>4</sub>F<sub>8</sub> molecules readily physisorbed at such low

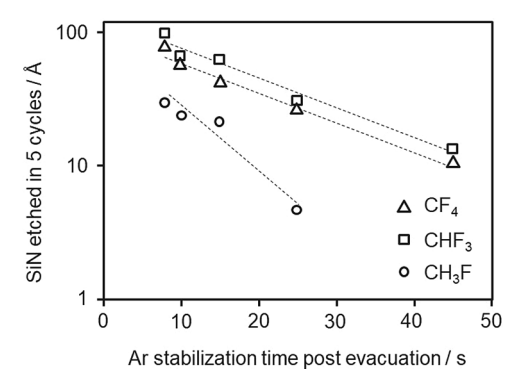


FIG. 30. SiN etched as a function of argon gas stabilization time between reactive gas evacuation and striking of argon plasma. Reprinted with permission from Sridhar et al., J. Vac. Sci. Technol. A 38, 043007 (2020). Copyright 2020, American Vacuum Society.



temperatures at the cooled surfaces. The  $C_4F_8$  pressure was roughly 20 mTorr. Etching is carried out using argon plasma with a low ion energy. Self-limiting etching of  $SiO_2$  is observed at  $-120\,^{\circ}C$  but not at  $-110\,^{\circ}C$ . The operating temperature of the process was increased to  $-90\,^{\circ}C$  by increasing the  $C_4F_8$  pressure from 20 to 40 mTorr and by reducing the purge step time, which reduced collision induced desorption. Other gases with high boiling points were considered to increase the process wafer temperature further. The benefit of this low temperature ALE process is that fluorocarbon polymer deposition on the reactor walls is significantly reduced, which should limit process drift.

#### D. Porous dielectric etching

Reducing the k-value of the dielectric material is one of the approaches to reduce signal delay in advanced logic devices. k-values below 2.5 can be achieved by creating interconnected pores, but radicals can diffuse into these pores during etching causing plasma-induced damage (PID) deep inside the material. Capillary condensation of reaction products<sup>13,55</sup> or etch gases<sup>56,57,59,60</sup> has been demonstrated to reduce the PID of low-k porous organosilicate (OSG). When SF<sub>6</sub> was used as the etch gas, PID was reduced due to a protective effect of etch by-products, which condense in the low-k material at -70 °C. 55 The addition of SiF<sub>4</sub> and O<sub>2</sub> further reduced PID due to enhanced SiO<sub>x</sub>F<sub>y</sub> passivation. The condensed phase is later desorbed during warm-up to room temperature combined with an additional annealing. The threshold temperature at which PID is meaningfully reduced depends on the pore size of low-k materials. 13 The temperature can be increased by using gases with higher boiling points. 56,57,59,60 Using C<sub>4</sub>F<sub>8</sub>, complete pore filling was achieved at −110 °C and negligible plasma-induced damage was demonstrated.<sup>56</sup> At this temperature, pore filling is far from complete in the case of pure SF<sub>6</sub>. 50 Only the pore sidewalls of the pores are covered by adsorbed SF<sub>6</sub> because capillary condensation starts with multilayer adsorption.<sup>5</sup> Chanson et al. introduced a specially designed new high boiling point organic reagent (HBPO), which was delivered into the vacuum chamber with a liquid injection system to increase the operating temperature further. 60 At a partial pressure of 3 mTorr, the onset of microcapillary condensation occurred at around +20 °C and the low-k matrix is filled at -20 °C as shown in Fig. 31.60 The composition of the molecule was not disclosed. Some VUV photodissociation of the BPO molecule causing a small increase in the k-value was observed.

### E. Radical etching

Nishino *et al.* demonstrated an interesting approach for the isotropic etching of  $SiO_2$  using a downstream plasma containing water and  $SF_6$ . The authors hypothesized that a condensed layer on the wafer is formed during processing since the  $SiO_2$  etching rate was found to increase by lowering the wafer temperature. The data are shown in Fig. 32. The possibility of a liquid film formation was supported by the gas analysis in the reaction chamber, which showed a large amount of HF, SO, and  $SO_2$  during the discharge of the gas mixture. It is possible that the liquid layer on the wafer contained  $H_2SO_4$  and  $H_2SO_3$ , which were produced by the reaction between  $SO_x$  and  $H_2O$ . These results indicate that it could be

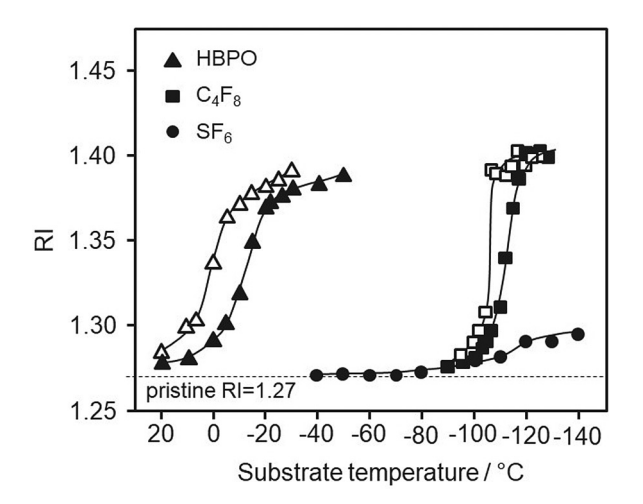


**FIG. 31.** Refractive index (RI) for adsorption–desorption cycles on porous oxide films for gas flows of SF<sub>6</sub>/HBPO = 30/4 SCCM at a pressure of 22.5 mTorr and with reference gases  $C_4F_8$  and SF<sub>6</sub> at a pressure of 7.5 mTorr. Adsorption is represented by full symbols and desorption by open symbols. Reprinted with permission from Chanson *et al.*, Sci. Rep. **8**, 1886 (2018). Copyright 2018 Author(s), licensed under a Creative Commons License.

possible to create liquid phase chemistry at the wafer surface when operating at low temperatures.

# F. Electron beam etching

Electron beam induced etching (EBIE) can be realized by adsorbing reactive gases at the surface and activating them with an electron beam. This method enables, in principle, maskless etching. Its versatility is, however, limited by the range of suitable precursor—substrate combinations. Martin  $et\ al.$  demonstrated in the case of NF3 that this challenge can be addressed by utilizing

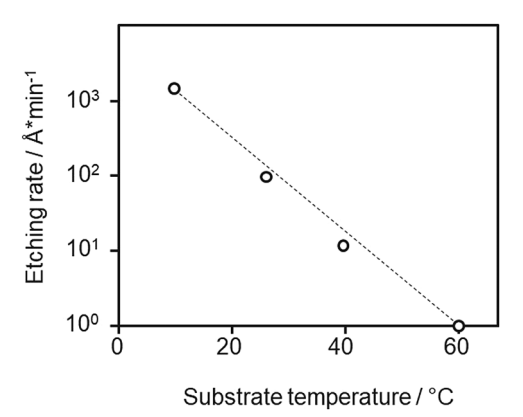


**FIG. 32.**  ${\rm SiO_2}$  etching rate as a function of wafer temperature. Reproduced with permission from Nishino *et al.*, J. Appl. Phys. **74**, 1345 (1993). Copyright 1993, AIP Publishing LLC.



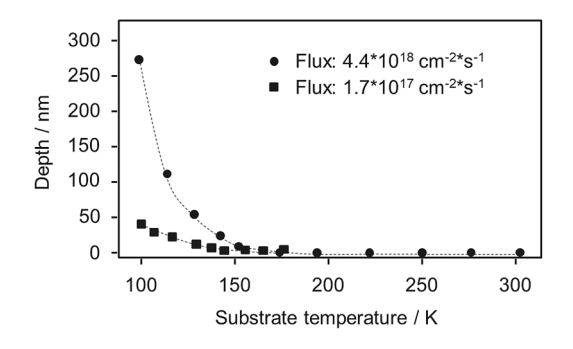


FIG. 33. Etch depth vs substrate temperature for NF<sub>3</sub>-mediated EBIE of silicon. Reprinted with permission from A. A. Martin and M. Toth, ACS Appl. Mater. Interfaces 6, 18457 (2014). Copyright 2014, American Chemical Society.

low surface temperatures.<sup>88</sup> While NF<sub>3</sub> satisfies most of the key requirements for EBIE such as a large electron dissociation cross section, high vapor pressure, relatively low toxicity, and hardware compatibility, it is not used in EBIE because it does create a high enough surface coverage at room temperature for many materials. Figure 33 shows an increase in the electron beam induced etching rate of silicon with NF<sub>3</sub> as the temperature is reduced. Physisorption energies between 0.062 and 0.064 eV were derived for two different NF3 fluxes. EBIE with NF3 was also demonstrated for SiO<sub>2</sub>, SiN, and SiC at -168 °C.

# G. Atomic layer deposition

ALD is increasingly used to protect the sidewall of high aspect ratio structures during etching. ALD is a sequence of at least two self-terminating gas-solid chemical surface reactions. It is desirable to deploy ALD in situ for cost reasons, which could be a challenge for low temperature etching. In principle, it should be possible to utilize physisorption in the first step. The conversion in the second step can be achieved via plasma assistance. The left panel of Fig. 34 shows the ideal process window for thermal ALD. 178,179 The lower temperature window is limited by either the condensation of precursors or low chemical reaction rates. For plasma assisted ALD, it should be possible to extend the process to lower surface temperatures as shown in the right panel. A temperature window should exist where pre-cursor molecules physisorb in one or several layers. Plasma provides the energy for the conversion reaction at low temperatures. Besides enabling in situ passivation during low temperature etch, this regime is expected to offer higher deposition rates thanks to faster saturation. Enhanced mass transport via surface diffusion should provide better conformality at shorter cycle times. Capillary condensation could be leveraged for the filling of high aspect ratio features. Precursors can be specially designed for physisorption to dissociate during activation into species, which provide high film quality and low contamination. For the adsorption to be self-terminating, the adsorbed material must not desorb from the surface during the purge step. 180 Physisorption is reversable, but at low enough temperatures and with highly polar molecules, it should be possible to suppress desorption in the time scale of the purge step.

Studies on ALD where step A explicitly uses physisorbed precursors are difficult to find. Horiike et al. realized poly-Si ALD by directing an ArF excimer laser onto a condensed Si<sub>2</sub>H<sub>6</sub> layer at −70 ° C and 50 mTorr. <sup>176</sup> Figure 35 shows the measured deposition rate as a function of surface temperature. The growth rate increases rapidly with decreasing substrate temperature. This temperature behavior shows that the Si<sub>2</sub>H<sub>6</sub> molecules are indeed physisorbed on the surface. The activation energy of 0.3 eV is in the range of typical o physisorption energies. At temperatures below -50 °C, the growth rate drops. At these temperatures, multilayer adsorption prevents the photodissociation products from reaching the surface. The authors were able to control the thickness of the physisorbed layer via pulsing frequency and pressure. The reaction rate of the first monolayer of Si<sub>2</sub>H<sub>6</sub> on the poly-Si surface is estimated to be about 40 about 40 discontinuous times as high compared with the second or third Si<sub>2</sub>H<sub>6</sub> layer. <sup>17</sup>

Low temperature plasma assisted ALD processes temperatures as low as 20 °C are subject of intense research.

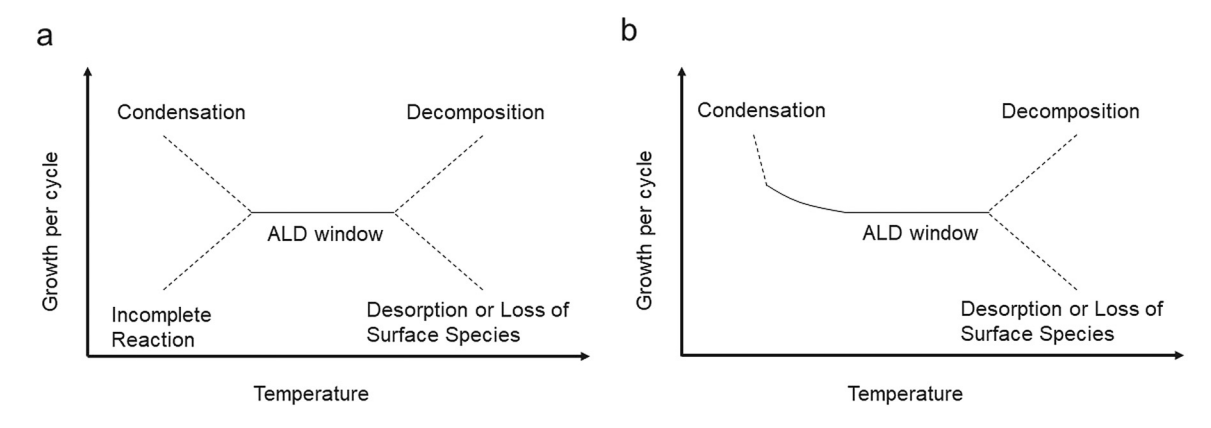


FIG. 34. Schematic of possible behavior for the ALD growth per cycle vs temperature for thermal ALD (a) and plasma assisted ALD (b). The graph on the left panel is reprinted with permission from S. M. George, Chem. Rev. 110, 111 (2010). Copyright 2010, American Chemical Society.

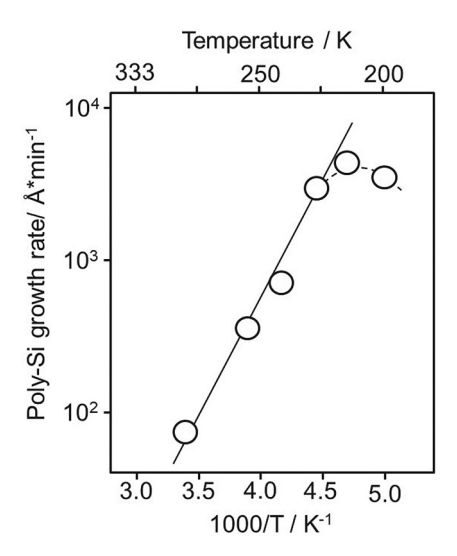


FIG. 35. Silicon growth rate plotted against substrate temperature. Reprinted with permission from Horiike et al., J. Vac. Sci. Technol. A 8, 1844 (1990). Copyright 1990, American Vacuum Society.

Table V is a list of low temperature ALD processes for metals and metal oxides. If physisorption plays a role at these temperatures, the growth per cycle (GPC) should increase as the temperature decreases. Indeed, most papers report a higher GPC at low

temperatures. ALD of Ta with TaCl<sub>5</sub> and atomic hydrogen shows the opposite trend with GPC ranging from 0.16 to 0.5 Å cycle at 25 °C to 1.67 Å/cycle at 250–400 °C.  $^{181}$  While this trend suggests chemisorption, the authors of this paper assumed that TaCl<sub>5</sub> is physisorbed at the surface. Among the systems in Table V, the mechanism of the temperature dependence of Al<sub>2</sub>O<sub>3</sub> ALD with Al (CH<sub>3</sub>)<sub>3</sub> and oxygen plasma has been studied in great detail. The reason for a higher GPC at low temperatures is an increased concentration of OH groups at the surface, which serve as the sites for the chemical adsorption of the precursor molecule. 180 For the other systems listed in Table V, detailed mechanism studies are not readily available. It is, therefore, impossible to conclude whether or not physisorption plays a role.

In summary, more work is needed to explore the potential of plasma assisted ALD in a regime where precursors predominantly physisorb at the surface. The pre-cursor molecules can be designed specifically to avoid film contamination. At the same time, the requirement to easily chemisorb at the surface is not important and can be relaxed.

#### **IV. SUMMARY**

Etching at lower water setching technology. It is characterized of as enhanced neutral adsorption via physisorption mass transport due to reduced chemical reactivity and possurface diffusion of molecules. Low temperature etch mechanisms are particularly useful for the etching of high aspect ratio features, which are critical technology drivers for 3D NAND and DRAM Reference

TABLE V. Examples of plasma assisted low substrate temperature ALD.

Film	Step A	Step B	Temperature °C	Comment	Reference
$Al_2O_3$	$Al(CH_3)_3$	O <sub>2</sub> plasma	25-300	Higher GPC at lower temperature	184
		-		Oxygen-rich films with a lower mass density and higher H	
				content at low temperatures	
			25-150	More -OH and C-related impurities at low temperature	186
				Chemisorption on OH groups	
			100-300	Higher GPC at lower temperature	189
$PtO_2$	$MeCpPtMe_3$	$O_2$ plasma	100-300	Higher GPC at low temperature	187
$Ta_2O_5$	$Ta(NMe_2)_5$	$O_2$ plasma	100-500	Higher GPC at the lowest and highest temperatures	182,183
				No carbon detected	
			100-225	Slightly higher GPC at lower temperature	185
				Higher H content at low temperature	
$HfO_2$	TEMAH	O <sub>2</sub> neutral	20-30	High quality amorphous film	190
		beam		GPC independent on purge time	
$Al_2O_3$	$Al(CH_3)_3$	$O_2$ plasma	25-400	Higher GPC at lower temperature partially attributed to lower	188
$TiO_2$	Ti(O¹Pr) <sub>4</sub>			density	
$Ta_2O_5$	$Ti(Cp^{Me})(O^{i}Pr)_{3}$				
	$TiCp*(OMe)_3$				
	$Ta(NMe_2)_5$				
Ta	$TaCl_5$	Atomic	25-400	Lower GPC for Ta at lower temperature	181
		hydrogen			
Ti	$TiCl_4$			Physisorption assumed	



memories. Future work should be focused on investigating ARDE at low temperatures to identify whether surface diffusion can be leveraged to etch faster at greater depth. This is of outmost importance for the extension of the 3D NAND memory roadmap.

In conventional etching, ARDE effect is not dependent on the absolute feature sizes. At low temperatures, surface diffusion may contribute meaningfully to the transport of molecules to the etch front. If this is the case, smaller features should etch faster than larger features with the same aspect ratio if the process is neutral flux limited. When features with different mask openings are etched, the resulting aspect ratio of the feature with smaller mask opening should be larger. This would effectively counteract ARDE. The effect can be used to decern whether surface diffusion is present. From a practical point of view, it is of special importance for extending planar DRAM devices via the shrinking of the diameter and increasing the height of the capacitor.

New gases should be explored to fully leverage the benefits of low temperature etching. The mechanisms that are responsible for the etching rate and ARDE effects are dependent on the adsorption and surface diffusion energies, which, in turn, are chemistry dependent. Molecules can be chosen, which physisorb at higher temperatures to simplify the hardware and to avoid process shifts due to the adsorption of background water. Because molecules physisorb directly from the gas phase without undergoing plasma dissociation, the evaluation of suitable gases is not complicated by plasma chemistry. It is, however, important to consider the effects of dissociated species on the process.

Capillary condensation limits temperatures at the low end. Heating from the plasma as well as ion, photon, and electron exposure suppress capillary condensation. When access by plasma is limited such as in horizontal features, gases may condense selectively. It is possible to imagine use cases for advanced 3D memories, which have vertical and horizontal features.

Finally, the etching of high aspect ratio features leverages increasingly sidewall passivation by ALD. It is, therefore, important to study ALD under the conditions of physisorption of gas molecules. This may require specially designed precursors.

# **ACKNOWLEDGMENTS**

The authors would like to thank Mark Wilcoxson, Gowri Kamarthy, Eric Hudson, Leonid Belau, and Mariusch Gregor at Lam Research and Steven George at the University of Colorado for valuable discussions.

#### **AUTHOR DECLARATIONS**

#### **Conflict of Interest**

The authors have no conflicts to disclose.

# **Author Contributions**

Thorsten Lill: Conceptualization (equal); Data curation (equal); Formal analysis (equal); Writing – original draft (equal). Ivan L. Berry: Conceptualization (equal); Formal analysis (equal); Software (equal); Writing – review & editing (equal). Meihua Shen: Data curation (equal); Writing – review & editing (equal). John Hoang: Data curation (equal); Writing – review & editing

(equal). Andreas Fischer: Formal analysis (equal); Writing – review & editing (equal). Theo Panagopoulos: Data curation (equal); Formal analysis (equal); Writing – review & editing (equal). Jane P. Chang: Conceptualization (equal); Formal analysis (equal); Writing – review & editing (equal). Vahid Vahedi: Conceptualization (equal); Formal analysis (equal); Funding acquisition (equal); Writing – review & editing (equal).

#### **DATA AVAILABILITY**

The data that support the findings of this study are available from the corresponding author upon reasonable request.

#### **REFERENCES**

- <sup>1</sup>T. Lill, V. Vahedi, and R. Gottscho, "Etching of semiconductor devices," in *Materials Science and Technology* (Wiley, New York, 2019).
- <sup>2</sup>S. Tachi, K. Tsujimoto, and S. Okudaira, Appl. Phys. Lett. **52**, 616 (1988).
- <sup>3</sup>S. Tachi, K. Tsujimoto, S. Arai, and T. Kure, J. Vac. Sci. Technol. A **9**, 796 (1991).
- <sup>4</sup>K. Tsujimoto, S. Okudaira, and S. Tachi, Jpn. J. Appl. Phys. 30, 3319 (1991).
- <sup>5</sup>M. Konuma, F. Banhart, F. Phillipp, and E. Bauser, Mater. Sci. Eng. B **4**, 265 (1989).
- <sup>6</sup>S. J. Pearton, C. R. Abernathy, F. Ren, J. R. Lothian, and R. F. Kopf, Plasma Chem. Plasma Process. **14**, 505 (1994).
- <sup>7</sup>E. S. Aydil, J. A. Gregus, and R. A. Gottscho, Rev. Sci. Instrum. **64**, 3572 (1993)
- <sup>8</sup>T. D. Bestwick, G. S. Oehrlein, and D. Angell, Appl. Phys. Lett. 57, 431 (1990).
- <sup>9</sup>K. Murakami, Y. Wakabayashi, K. Minami, and M. Esashi, Proc. IEEE Micro Electro Mech. Syst. 65 (1993).
- <sup>10</sup>R. Chanson, S. Tahara, K. Vanstreels, and J.-F. de Marneffe, Plasma Res. Express 1, 015006 (2019).
- <sup>11</sup>R. Chanson, R. Dussart, T. Tillocher, P. Lefaucheux, C. Dussarrat, and J.-F. de Marneffe, Front. Chem. Sci. Eng. 13, 511 (2019).
- <sup>12</sup>M. A. Blauw, T. Zijlstra, R. A. Bakker, and E. van der Drift, J. Vac. Sci. Technol. B 18, 3453 (2000).
- $^{13}$ L. Zhang, R. Ljazouli, P. Lefaucheux, T. Tillocher, R. Dussart, Y. Mankelevich,  $^{12}$ J.-F. de Marneffe, S. de Gendt, and M. Baklanov, Electrochem. Solid State Lett. 2, N131 (2013).
- <sup>14</sup>H. Jansen, M. de Boer, R. Legtenberg, and M. Elwenspoek, J. Micromech. Microeng. 5, 115 (1995).
- <sup>15</sup>H. Jansen, M. de Boer, J. Burger, R. Legtenberg, and M. Elwenspoek, Microelectron. Eng. 27, 475 (1995).
- <sup>16</sup>M. Esashi, M. Takinami, Y. Wakabayashi, and K. Minami, J. Micromech. Microeng. 5, 5 (1995).
- <sup>17</sup>J. W. Bartha, J. Greschner, M. Puech, and P. Maquin, Microelectron. Eng. 27, 453 (1995).
- <sup>18</sup>T. Wells, M. M. El-Gomati, and J. Wood, J. Vac. Sci. Technol. B **15**, 434 (1997).
- <sup>19</sup>T. Chevolleau, P. Y. Tessier, C. Cardinaud, and G. Turban, J. Vac. Sci. Technol. A 15, 2661 (1997).
- <sup>20</sup>H. Jansen, M. de Boer, R. Wiegerink, N. Tas, E. Smulders, C. Neagu, and M. Elwenspoek, Microelectron. Eng. 35, 45 (1997).
- <sup>21</sup>M. J. M. Vugts, G. L. J. Verschueren, M. F. A. Eurlings, L. J. F. Hermans, and
- H. C. W. Beijerinck, J. Vac. Sci. Technol. A 14, 2766 (1996).
   22S. Aachboun and P. Ranson, J. Vac. Sci. Technol. A 17, 2270 (1999).
- <sup>23</sup>T. Zijlstra, E. van der Drift, M. J. A. de Dood, E. Snoeks, and A. Polman, J. Vac. Sci. Technol. B 17, 2734 (1999).
- <sup>24</sup>H. Jansen, M. De Boer, H. Wensink, B. Kloeck, and M. Elwenspoek, Microelectron. J. **32**, 769 (2001).
- <sup>25</sup>G. Craciun, M. A. Blauw, E. van der Drift, P. M. Sarro, and P. J. French, J. Micromech. Microeng, **12**, 390 (2002).

- 26 M. W. Pruessner, W. S. Rabinovich, T. H. Stievater, D. Park, and J. W. Baldwin, J. Vac. Sci. Technol. B 25, 21 (2007).
- <sup>27</sup>J. Pereira, L. E. Pichon, R. Dussart, C. Cardinaud, C. Y. Duluard, E. H. Oubensaid, P. Lefaucheux, M. Boufnichel, and P. Ranson, Appl. Phys. Lett. 94, 071501 (2009).
- <sup>28</sup>N. Chekurov, K. Grigoras, A. Peltonen, S. Franssila, and I. Tittonen, Janotechnology 20, 065307 (2009).
- <sup>29</sup>T. Maruyama, T. Narukage, R. Onuki, and N. Fujiwara, J. Vac. Sci. Technol. B
- 30 T. Maruyama, T. Narukage, R. Onuki, and N. Fujiwara, J. Vac. Sci. Technol. B 28, 862 (2010).
- 31 R. Dussart, T. Tillocher, P. Lefaucheux, and M. Boufnichel, J. Phys. D: Appl. Phys. 47, 123001 (2014).
- 32M. J. de Boer, J. G. E. Gardeniers, H. V. Jansen, E. Smulders, M.-J. Gilde, G. Roelofs, J. N. Sasserath, and M. Elwenspoek, J. Microelectromech. Syst. 11, 385 (2002).
- 33M. Puech and P. Maquin, Appl. Surf. Sci. 100-101, 579 (1996).
- 34S. Aachboun, P. Ranson, C. Hilbert, and M. Boufnichel, J. Vac. Sci. Technol. A
- 35 M. J. de Boer, R. Tjerkstra, J. W. Berenschot, H. Jansen, G. J. Burger, J. G. E. Gardeniers, M. Elwenspoek, and A. van den Berg, J. Microelectromech. Syst. 9, 94 (2000).
- <sup>36</sup>R. Dussart et al., J. Micromech. Microeng. **14**, 190 (2004).
- 37M. Boufnichel, S. Aachboun, F. Grangeon, P. Lefaucheux, and P. Ranson, Vac. Sci. Technol. B 20, 1508 (2002).
- <sup>38</sup>M. Boufnichel, S. Aachboun, P. Lefaucheux, and P. Ranson, J. Vac. Sci. Technol, B 21, 267 (2003).
- <sup>39</sup>M. Boufnichel, P. Lefaucheux, S. Aachboun, R. Dussart, and P. Ranson, Microelectron. Eng. 77, 327 (2005).
- <sup>40</sup>I. W. Rangelow, J. Vac. Sci. Technol. A **21**, 1550 (2003).
- <sup>41</sup>H. Jansen, M. de Boer, S. Unnikrishnan, M. Louwerse, and M. Elwenspoek, . Micromech. Microeng. 19, 033001 (2009).
- <sup>42</sup>M. D. Henry, C. Welch, and A. Scherer, J. Vac. Sci. Technol. A 27, 1211
- 43T. Tillocher, R. Dussart, X. Mellhaoui, P. Lefaucheux, N. Mekkakia Maaza, P. Ranson, M. Boufnichel, and L. J. Overzet, J. Vac. Sci. Technol. A 24, 1073
- 44R. Dussart, X. Mellhaoui, T. Tillocher, P. Lefaucheux, M. Boufnichel, and P. Ranson, Microelectron. Eng. 84, 1128 (2007).
- 45G. Marcos, A. Rhallabi, and P. Ranson, J. Vac. Sci. Technol. B 22, 1912 (2004).
- <sup>46</sup>G. Marcos, A. Rhallabi, and P. Ranson, Appl. Surf. Sci. 254, 3576 (2008).
- <sup>47</sup>L. Sainiemia and S. Franssila, J. Vac. Sci. Technol. B 25, 801 (2007).
- <sup>48</sup>C. Y. Duluard, R. Dussart, T. Tillocher, L. E. Pichon, P. Lefaucheux, M. Puech, and P. Ranson, Plasma Sources Sci. Technol. 17, 045008 (2008).
- 49 A. F. Isakovic, K. Evans-Lutterodt, D. Elliott, A. Stein, and J. B. Warren, J. Vac. Sci. Technol. A 26, 1182 (2008).
- 50 T. Tillocher, W. Kafrouni, J. Ladroue, P. Lefaucheux, M. Boufnichel, P. Ranson, and R. Dussart, J. Micromech. Microeng. 21, 085005 (2011).
- 51 A. Kamto, R. Divan, A. V. Sumant, and S. L. Burkett, J. Vac. Sci. Technol. A 28, 719 (2010).
- 52 F. Jiang, A. Keating, M. Martyniuk, K. Prasad, L. Faraone, and J. M. Dell, . Micromech. Microeng. 22, 095005 (2012).
- 53H. V. Jansen, M. J. de Boer, K. Ma, M. Girones, S. Unnikrishnan, M. C. Louwerse, and M. C. Elwenspoek, J. Micromech. Microeng. 20, 075027
- 54C. Y. Duluard, P. Ranson, L. E. Pichon, J. Pereira, E. H. Oubensaid, P. Lefaucheux, M. Puech, and R. Dussart, J. Micromech. Microeng. 21, 065015
- 55L. Zhang, R. Ljazouli, P. Lefaucheux, T. Tillocher, R. Dussart, Y. A. Mankelevich, J.-F. de Marneffe, S. de Gendt, and M. R. Baklanov, ECS Solid State Lett. 2, N5 (2013).
- 56L. Zhang et al., J. Phys. D: Appl. Phys. 49, 175203 (2016).

- <sup>57</sup>Q. L. Zhang, S. Tinck, J.-F. de Marneffe, L. Zhang, and A. Bogaerts, Appl. Phys. Lett. 111, 173104 (2017).
- <sup>58</sup>F. Iacopi, J. H. Choi, K. Terashima, P. M. Rice, and G. Dubois, Phys. Chem. Chem. Phys. 13, 3634 (2011).
- <sup>59</sup>F. Leroy et al., J. Phys. D: Appl. Phys. **48**, 435202 (2015).
- 60 R. Chanson, L. Zhang, S. Naumov, Y. A. Mankelevich, T. Tillocher, P. Lefaucheux, R. Dussart, S. De Gendt, and J.-F. de Marnefe, Sci. Rep. 8, 1886
- <sup>61</sup>K. Shinoda, N. Miyoshi, H. Kobayashi, Y. Hanaoka, K. Kawamura, M. Izawa, K. Ishikawa, and M. Hori, Proc. SPIE 10589, 105890I (2018).
- 62K. Shinoda, N. Miyoshi, H. Kobayashi, M. Izawa, T. Saeki, K. Ishikawa, and M. Hori, J. Vac. Sci. Technol. A 37, 051002 (2019).

  <sup>63</sup>G. Antoun, P. Lefaucheux, T. Tillocher, R. Dussart, K. Yamazaki, K. Yatsuda,
- J. Faguet, and K. Maekawa, Appl. Phys. Lett. 115, 153109 (2019).
- 64S. Dallorto, A. Goodyear, M. Cooke, J. E. Szornel, C. Ward, C. Kastl, A. Schwartzberg, I. W. Rangelow, and S. Cabrini, Plasma Processes Polym. 16,
- 65S. Dallorto, M. Lorenzon, J. Szornel, A. Schwartzberg, A. Goodyear, M. Cooke, M. Hofmann, I. W. Rangelow, and S. Cabrini, J. Vac. Sci. Technol. B 37, 051805
- 66S. Sridhar, P. L. G. Ventzek, and A. Ranjan, J. Vac. Sci. Technol. A 38, 043007
- 67G. Antoun, T. Tillocher, P. Lefaucheux, J. Faguet, K. Maekawa, and R. Dussart, ci. Rep. 11, 357 (2021).
- 68G. Antoun et al., J. Vac. Sci. Technol. A 40, 052601 (2022).
- 69D. L. Olynick, E. H. Anderson, B. Harteneck, and E. Veklerov, J. Vac. Sci. Technol. B 19, 2896 (2001).
- 70 Z. Liu, Y. Wu, B. Harteneck, and D. Olynick, Nanotechnology 24, 015305 (2013).
- 71C. Peroz, S. Dhuey, M. Volger, Y. Wu, D. Olynick, and S. Cabrini, Nanotechnology 21, 445301 (2010).
- 72Y. Wu, D. L. Olynick, A. Goodyear, C. Peroz, S. Dhuey, X. Liang, and S. Cabrini, Microelectron. Eng. **88**, 2785 (2011). **73**C. C. Welch *et al.*, Proc. SPIE **8700**, 870002 (2013).
- 74Z. Li, Y. Chen, X. Zhu, M. Zheng, F. Dong, P. Chen, L. Xu, W. Chu, and H. Duan, Nanotechnology 27, 365302 (2016).
- 75A. Smyrnakis, E. Almpanis, V. Constantoudis, N. Papanikolaou, and E. Gogolides, Nanotechnology 26, 085301 (2015).
- <sup>76</sup>A. Smyrnakis, A. Zeniou, K. Awsiuk, V. Constantoudis, and E. Gogolides, Front. Chem. Sci. Eng. 13, 475 (2019).
- 77 I. W. Rangelow et al., J. Vac. Sci. Technol. B 34, 06K202 (2016).
- <sup>78</sup>R. K. Dey, H. Ekinci, and B. Cui, J. Vac. Sci. Technol. B **38**, 012207 (2020).
- <sup>79</sup>S. N. Hsiao, K. Nakane, T. Tsutsumi, K. Ishikawa, M. Sekine, and M. Hori, Appl. Surf. Sci. 542, 148550 (2021).
- 80S. N. Hsiao, T. T. N. Nguyen, T. Tsutsumi, K. Ishikawa, M. Sekine, and M. Hori, Coatings 11, 1535 (2021).
- 81 Semiconductor Engineering 2018: Cryogenic Etch Re-Emerges (semiengineering.com).
- 82 E. Hudson and F. Roberts, U.S. patent 0286707 A1 (4 October 2018).
- 83R. Takeda, R. Takashima, and Y. Ooya, U.S. patent 9659789 B2 (23 May
- 84R. A. Gottscho, C. W. Jurgensen, and D. J. Vitkavage, J. Vac. Sci. Technol. B
- 85 F. London, Z. Phys. 63, 245 (1930) [Trans. Faraday Soc. 33, 8b (1937)].
- <sup>86</sup>D. Beaglehole and H. K. Christenson, J. Phys. Chem. **96**, 3395 (1992).
- 87 I. Toyoshima and G. A. Somorjai, Catal. Rev. 19, 105 (1979).
- 88 A. A. Martin and M. Toth, ACS Appl. Mater. Interfaces 6, 18457 (2014).
- 89 T. Chowdhury, R. Hidayat, T. R. Mayangsari, J. Gu, H.-L. Kim, J. Jung, and W.-J. Lee, J. Vac. Sci. Technol. A 37, 021001 (2019).
- 90 T. Chowdhury, R. Hidayat, H.-L. Kim, T. R. Mayangsari, S. Cho, S. Park, J. Jung, and W.-J. Lee, Appl. Surf. Sci. 554, 149481 (2021).
- 91 E. Cheng and G. S. Hwang, Appl. Surf. Sci. **543**, 148557 (2021).
- 92D. B. Graves and D. Humbird, Appl. Surf. Sci. 192, 72 (2002).

- 93D. B. Graves and P. Brault, J. Phys. D: Appl. Phys. 42, 194011 (2009).
- 94G. S. Oehrlein and S. Hamaguchi, Plasma Sources Sci. Technol. 27, 023001 (2018).
- 95G. Davis and R. A. Gottscho, J. Appl. Phys. 54, 3080 (1983).
- <sup>96</sup>G. Cunge, R. Ramos, D. Vempaire, M. Touzeau, M. Neijbauer, and N. Sadeghi, J. Vac. Sci. Technol. A 27, 471 (2009).
- 97 H. F. Winters and J. W. Coburn, Appl. Phys. Lett. 34, 70 (1979).
- 98J. W. Coburn and H. F. Winters, J. Appl. Phys. 50, 3189 (1979).
- 99S. Tinck, E. C. Neyts, and A. Bogaerts, J. Phys. Chem. C 118, 30315 (2014).
- 100 R. Gomer, Rep. Prog. Phys. 53, 917 (1990).
- 101 T. Ohiwa, K. Horioka, T. Arikado, I. Hasegawa, and H. Okano, Jpn. J. Appl. Phys. 31, 405 (1992).
- 102W.-H. Kim, D. Sung, S. Oh, J. Woo, S. Lim, H. Lee, and S. F. Bent, J. Vac. Sci. Technol. A 36, 01B104 (2018).
- 103G. S. Oehrlein and Y. Kurogi, Mater. Sci. Eng. R 24, 153 (1998).
- 104 J. D. Beckerle, Q. Y. Yang, A. D. Johnson, and S. T. Ceyers, J. Chem. Phys. 86, 7236 (1987).
- 105 J. D. Beckerle, A. D. Johnson, and S. T. Ceyer, Phys. Rev. Lett. 62, 685 (1989).
- 106 J. D. Beckerle, A. D. Johnson, Q. Y. Yang, and S. T. Ceyer, J. Chem. Phys. 91, 5756 (1989).
- <sup>107</sup>J. Royer, P. Y. Tessier, B. Grolleau, and G. Turban, J. Vac. Sci. Technol. A 14, 234 (1996).
- <sup>108</sup>D. J. Oostra, A. Haring, and A. E. De Vries, Nucl. Instrum. Methods Phys. Res. B 16, 364 (1986).
- <sup>109</sup>P. G. M. Sebel, L. J. F. Hermans, and H. C. W. Beijerinck, J. Vac. Sci. Technol. A 18, 2090 (2000).
- <sup>110</sup>H. F. Winters, J. Vac. Sci. Technol. A 3, 700 (1985).
- 1111 J. Pelletier, J. Phys. D: Appl. Phys. 20, 858 (1987).
- 112 A. Bensaoula, E. Grossman, and A. Ignatiev, J. Appl. Phys. 62, 4587 (1987).
- 113P. G. M. Sebel, L. J. F. Hermans, and H. C. W. Beijerinck, J. Vac. Sci. Technol. A 17, 3368 (1999).
- 114Z. Paszti, O. Hakkel, T. Keszthelyi, A. Berko, N. Balazs, I. Bako, and L. Guczi, Langmuir 26, 16312 (2010).
- 115 T. Meguro, M. Hamagaki, S. Modaressi, T. Hara, Y. Aoyagi, M. Ishii, and Y. Yamamoto, Appl. Phys. Lett. 56, 1552 (1990).
- 116 S. Veprek and F. A. Sarott, Plasma Chem. Plasma Process. 2, 233 (1982).
- <sup>117</sup>R. O. Martinez, T. R. Verhey, P. K. Boyer, and J. J. Rocca, J. Vac. Sci. Technol. B **6**, 1581 (1988).
- <sup>118</sup>H. P. Gillis, J. L. Clemons, and J. P. Chamberlain, J. Vac. Sci. Technol. B 10, 2729 (1992).
- <sup>119</sup>F. A. Houle, Phys. Rev. B **39**, 10120 (1989).
- 120 M. C. Shih, M. B. Freiler, G. Haase, R. Scarmozzino, and R. M. Osgood, Appl. Phys. Lett. 61, 828 (1992).
- 121 B. Li, U. Streller, H-P Krause, I. Twesten, and N. Schwentner, J. Appl. Phys. 77, 350 (1995).
- 122 R. G. Livesay, "Flow of gases through tubes and orifices," in *Foundations of Vacuum Science and Technology*, edited by J. M. Lafferty (Wiley, New York, 1998), Chap. 2.
- <sup>123</sup>M. Knudsen, Ann. Phys. **333**, 75 (1909).
- <sup>124</sup>L. Wu, Appl. Phys. Lett. **93**, 253103 (2008).
- <sup>125</sup>J. C. Maxwell, The Scientific Papers of James Clerk Maxwell (C. J. Clay & Sons, 1890), Vol. 2.
- 126<sub>L</sub>. B. Loeb, The Kinetic Theory of Gases, 2nd ed. (McGraw-Hill Book Company, 1934).
- 127 J. W. Coburn and H. F. Winters, Appl. Phys. Lett. 55, 2730 (1989).
- <sup>128</sup>H. A. Lorentz, Lectures on Theoretical Physics (Macmillan, London, 1927), Vol. 1, Chap. 3.
- 129 P. C. Carman and F. A. Raal, Proc. R. Soc. London A 209, 38 (1951).
- 130J. F. O'Hanlon, A User's Guide to Vacuum Technology, 3rd ed. (John Wiley & Sons, 2003).
- <sup>131</sup>P. Clausing, J. Vac. Sci. Technol. **8**, 636 (1971).
- 132 K. Miyabe and G. Guiochon, J. Chromatogr. A 1217, 1713 (2010).
- <sup>133</sup>I. Medved and R. Cerny, Microporous Mesoporous Mater. **142**, 405 (2011).

- 134X. Li, S. Liu, J. Li, X. Tan, Y. Li, and F. Wu, Energies 13, 6323 (2020).
- 135W. Li, D. Wang, and J. G. Wang, J. Nat. Gas Sci. Eng. 101, 104508 (2022).
- <sup>136</sup>E. R. Gilliland, R. F. Baddour, G. P. Perkinson, and K. J. Sladek, Ind. Eng. Chem. Fundam. 13, 95 (1974).
- 137 J. L. Brand, M. V. Arena, A. A. Deckert, and S. M. George, J. Chem. Phys. 92, 5136 (1990).
- 138 M. V. Arena, A. A. Deckert, J. L. Brand, and S. M. George, J. Phys. Chem. 94, 6792 (1990).
- <sup>139</sup>C. H. Mak, B. G. Koehler, and S. M. George, J. Vac. Sci. Technol. A 6, 856 (1988).
- 140 E. D. Westre, M. V. Arena, A. A. Deckert, J. L. Brand, and S. M. George, Surf. Sci. 233, 293 (1990).
- 141 M. V. Arena, E. D. Westre, and S. M. George, J. Chem. Phys. 94, 4001 (1991).
- 142 D. A. King, J. Vac. Sci. Technol. 17, 241 (1980).
- 143A. A. Deckert, J. L. Brand, M. V. Arena, and S. M. George, J. Vac. Sci. Technol. A 6, 794 (1988).
- <sup>144</sup>S. Brunauer, P. H. Emmett, and E. Teller, J. Am. Chem. Soc. **60**, 309 (1938).
- 145 I. Langmuir, J. Am. Chem. Soc. 40, 1361 (1918).
- 146Handbook of Chemistry and Physics Online: Vapor pressure of compounds and elements, Vapor Pressure of Compounds and Elements (chemnetbase.com).
  147C. B. Mullins and J. W. Coburn, J. Appl. Phys. 76, 7562 (1994).
- 148P. C. Carman and P. Le R. Malherbe, Proc. Math. Phys. Eng. Sci. 203, 165 (1950).
- 149Y. Horiguchi, R. R. Hudgins, and P. L. Silveston, Can. J. Chem. Eng. 49, 76 (1971).
- <sup>150</sup>K. S. W. Sing; D, H. Everett, R. A. W. Haul, L. Moscou, R. A. Pierotti, J. Rouquerol, and T. Siemieniewska, Pure Appl. Chem. 57, 603 (1985).
- <sup>151</sup>L. R. Fisher and J. N. Israelachvili, Nature 277, 548 (1979).
- <sup>152</sup>L. R. Fisher, R. A. Gamble, and J. Middlehurst, Nature **290**, 575 (1981).
- 153 J. H. Simons and J. W. Bouknight, J. Am. Chem. Soc. 54, 129 (1932).
- 154N. B. Hannay and C. P. Smyth, J. Am. Chem. Soc. 68, 171 (1946).
- 155S. A. Clough, Y. Beers, G. P. Klein, and L. S. Rothman, J. Chem. Phys. 59, 2254 (1973).
- 2254 (1973).

  156 X. Mellhaoui, R. Dussart, T. Tillocher, P. Lefaucheux, P. Ranson, M. Boufnichel, and L. J. Overzet, J. Appl. Phys. 98, 104901 (2005).
- M. Boufnichel, and L. J. Overzet, J. Appl. Phys. 98, 104901 (2005).

  Disparition of the control of the control
- 158<sub>H.</sub> S. Booth and R. A. Osten, J. Am. Chem. Soc. **67**, 1092 (1945).
- 159 B. Wu, A. Kumar, and S. Pamarthy, J. Appl. Phys. 108, 051101 (2010).
- <sup>160</sup>M. J. Walker, Proc. SPIE **4407**, 89 (2001).
- <sup>161</sup>S.-B. Jo, M.-W. Lee, S.-G. Lee, E.-H. Lee, S.-G. Park, and B.-H. Oh, J. Vac. Sci. Technol. A 23, 905 (2005).
- 162 T. Tillocher, R. Dussart, L. J. Overzet, X. Mellhaoui, P. Lefaucheux, M. Boufnichel, and P. Ranson, J. Electrochem. Soc. 155, D187 (2008).
- 163R. Dussart, P. Lefaucheux, X. Mellhaoui, L. J. Overzet, P. Ranson, T. Tillocher, and M. Boufnichel, U.S. patent 8,012,365 B2 (6 December 2011).
- <sup>164</sup>D. Kim, E. A. Hudson, D. Cooperberg, E. Edelberg, and M. Srinivasan, Thin Solid Films 515, 4874 (2007).
- 165 T. Iwase, K. Yokogawa, and M. Mori, Jpn. J. Appl. Phys. 57, 06JC03 (2018).
- 166T. Iwase, N. Kofuji, K. Yokogawa, and M. Mori, Jpn. J. Appl. Phys. 58, SEEB04 (2019).
- 167 T. Iwase, K. Yokogawa, and M. Mori, Jpn. J. Appl. Phys. 56, 06HB04 (2017).
- 168 T. Iwase, M. Matsui, K. Yokogawa, T. Arase, and M. Mori, Jpn. J. Appl. Phys. 55, 06HB02 (2016).
- 169 H. Nishino, N. Hayasaka, and H. Okano, J. Appl. Phys. 74, 1345 (1993).
- <sup>170</sup>T. Hayashi, K. Ishikawa, M. Sekine, M. Hori, A. Kono, and K. Suu, Jpn. J. Appl. Phys. 51, 016201 (2012).
- <sup>171</sup>Y. J. Gill, D. S. Kim, H. S. Gil, K. H. Kim, Y. J. Jang, Y. E. Kim, and G. Y. Yeom, Plasma Process. Polym. **18**, 2100063 (2021).
- 172H. Ogawa, T. Arai, M. Yanagisawa, T. Ichiki, and Y. Horiike, Jpn. J. Appl. Phys. 41, 5349 (2002).
- <sup>173</sup>W. O. Lee *et al.*, Sci. Rep. **12**, 5703 (2022).

- 174S. Huang, C. Huard, S. Shim, S. K. Nam, I. C. Song, S. Li, and M. J. Kushner, J. Vac. Sci. Technol. A 37, 031304 (2019).
- 175 K. J. Kanarik, T. Lill, E. A. Hudson, S. Sriraman, S. Tan, J. Marks, V. Vahedi, and R. A. Gottscho, J. Vac. Sci. Technol. A 33, 020802 (2015).
- 176 Y. Horiike, T. Tanaka, M. Nakano, S. Iseda, H. Sakaue, A. Nagata, H. Shindo,
- S. Miyazaki, and M. Hirose, J. Vac. Sci. Technol. A 8, 1844 (1990). 177H. Sakaue, S. Iseda, K. Asami, J. Yamamoto, M. Hirose, and Y. Horiike, Jpn. J. Appl. Phys. 29, 2648 (1990).
- 178<sub>S. M. George, Chem. Rev. 110, 111 (2010).</sub>
- 179G. S. Oehrlein, D. Metzler, and C. Li, ECS J. Solid State Sci. Technol. 4, N5041 (2015).
- <sup>180</sup>R. L. Puurunen, J. Appl. Phys. **97**, 121301 (2005).
- 181 S. M. Rossnagel, A. Sherman, and F. Turner, J. Vac. Sci. Technol. B 18, 2016
- 182 W. J. Maeng, S.-J. Park, and H. Kim, J. Vac. Sci. Technol. B 24, 2276 (2006).
- 183W. J. Maeng and H. Kim, Electrochem. Solid-State Lett. 9, G191 (2006).

- 184 J. L. van Hemmen, S. B. S. Heil, J. H. Klootwijk, F. Roozeboom, C. J. Hodson, M. C. M. van de Sanden, and W. M. M. Kessels, J. Electrochem. Soc. 154, G165
- 185 S. B. S. Heil, F. Roozeboom, M. C. M. van de Sanden, and W. M. M. Kessels, J. Vac. Sci. Technol. A 26, 472 (2008).
- 186 E. Langereis, J. Keijmel, M. C. M. van de Sanden, and W. M. M. Kessels, Appl. Phys. Lett. **92**, 231904 (2008). <sup>187</sup>H. C. M. Knoops, A. J. M. Mackus, M. E. Donders, M. C. M. van de Sanden,
- P. H. L. Notten, and W. M. M. Kessels, Electrochem. Solid-State Lett. 12, G34
- Sanden, and W. M. M. Kessels, J. Electrochem. Soc. 157, P66 (2010).

  189V. Vandalon and W. M. M. Kessels, Appl. Phys. Lett. 108, 011607
- 190B. Ge, D. Ohori, Y. H. Chen, T. Ozaki, K. Endo, Yiming Li, J.-H. Tarng, and S. Samukawa, J. Vac. Sci. Technol. A 40, 022405 (2022).